Article

Immunity

Antibodies and complement are key drivers of thrombosis

Graphical abstract

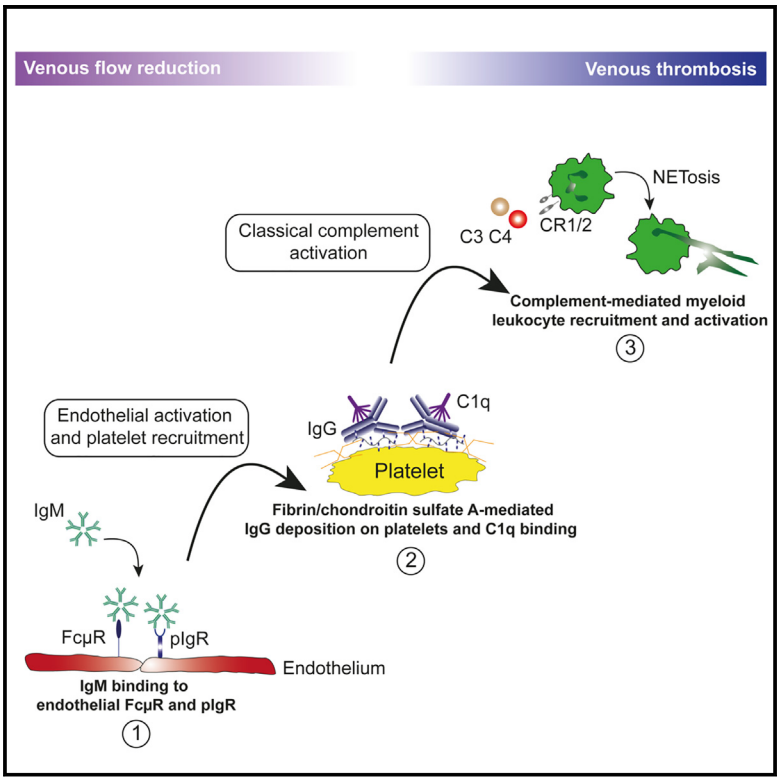

Highlights

- Antibodies are key drivers of thrombosis, irrespective of their antigen specificity
- IgM binds endothelial FcμR and pIgR, starting platelet recruitment to the vessel wall
- IgG locates to fibrin on activated platelets and activates classical complement
- Therapeutic complement inhibition limits thrombosis without compromising hemostasis

Authors

Konstantin Stark, Badr Kilani, Sven Stockhausen, ..., Bernd Engelmann, Admar Verschoor, Steffen Massberg

Correspondence

konstantin.stark@med.uni-muenchen.de (K.S.), admar.verschoor@tum.de (A.V.)

In brief

Conventional anticoagulant therapies to prevent thrombosis also carry inherent bleeding risks. Identifying that antibodies and complement are key drivers of venous thrombosis in mice, Stark et al. not only find hallmarks of the mechanism preserved in humans but also show that therapeutic complement inhibition prevents thrombosis without negatively impacting hemostasis.

Stark et al., 2024, Immunity 57, 2140–2156
September 10, 2024
https://doi.org/10.1016/j.immuni.2024.08.007

CellPress

CellPress
OPEN ACCESS

Immunity

Article

Antibodies and complement are key drivers of thrombosis

Konstantin Stark,[1,2,3,25,27,*] Badr Kilani,[1,2,3,25] Sven Stockhausen,[1,2,3,25] Johanna Busse,[1,3] Irene Schubert,[1,3] Thuy-Duong Tran,[1,3] Florian Gaertner,[1,2,3,4] Alexander Leunig,[1,2,3] Kami Pekayvaz,[1,2,3] Leo Nicolai,[1,2,3] Valeria Fumagalli,[5,6] Julia Stermann,[1,2,3] Felix Stephan,[1,2,3] Christian David,[7] Martin B. Müller,[3,8] Birgitta Heyman,[9] Anja Lux,[10,11] Alexandra da Palma Guerreiro,[12,13,14] Lukas P. Frenzel,[12,13,14] Christoph Q. Schmidt,[15] Arthur Dopler,[15] Markus Moser,[16,17] Sue Chandraratne,[1,3] Marie-Luise von Brühl,[1,3] Michael Lorenz,[1,3] Thomas Korff,[18] Martina Rudelius,[19] Oliver Popp,[20,21] Marieluise Kirchner,[20,21] Philipp Mertins,[20,21] Falk Nimmerjahn,[10,11] Matteo Iannacone,[5,6] Markus Sperandio,[7] Bernd Engelmann,[22] Admar Verschoor,[23,24,25,26,*] and Steffen Massberg[1,2,3,25,26]

[1]Medizinische Klinik und Poliklinik I, University Hospital, LMU Munich, Munich, Germany
[2]German Center for Cardiovascular Research (DZHK), partner site Munich Heart Alliance, Munich, Germany
[3]Walter-Brendel Center of Experimental Medicine, Faculty of Medicine, LMU Munich, Munich, Germany
[4]Institute of Science and Technology Austria, Klosterneuburg, Austria
[5]Division of Immunology, Transplantation, and Infectious Diseases, IRCCS San Raffaele Scientific Institute, Milan, Italy
[6]Vita-Salute San Raffaele University, Milan, Italy
[7]Institute for Cardiovascular Physiology and Pathophysiology, Walter Brendel Center for Experimental Medicine, Biomedical Center (BMC) LMU Munich, Munich, Germany
[8]Department of Anaesthesiology, University Hospital, LMU Munich, Munich, Germany
[9]Department of Medical Biochemistry and Microbiology, Uppsala University, Uppsala, Sweden
[10]Department of Biology, Institute of Genetics, Friedrich-Alexander University Erlangen-Nürnberg, Erlangen, Germany
[11]Medical Immunology Campus Erlangen (MICE), Friedrich-Alexander University Erlangen-Nürnberg (FAU), Erlangen, Germany
[12]Department I of Internal Medicine, University Hospital Cologne, Cologne 50937, Germany
[13]Center of Integrated Oncology ABCD, University Hospital of Cologne, Cologne, Germany
[14]Cologne Excellence Cluster on Cellular Stress Responses in Aging-Associated Diseases (CECAD), University of Cologne, Cologne 50937, Germany
[15]Institute of Experimental and Clinical Pharmacology, Toxicology and Pharmacology of Natural Products, University of Ulm Medical Center, Ulm, Germany
[16]Department of Molecular Medicine, Max-Planck-Institute of Biochemistry, Martinsried, Germany
[17]Institute of Experimental Hematology, TranslaTUM, Klinikum rechts der Isar der Technischen Universität München, Munich, Germany
[18]Division of Cardiovascular Physiology, Institute of Physiology and Pathophysiology, Heidelberg University, Heidelberg, Germany
[19]Institute of Pathology, Ludwig-Maximilian University, Munich, Germany
[20]Max Delbrück Center for Molecular Medicine (MDC) and Berlin Institute of Health (BIH), Berlin, Germany
[21]German Center for Cardiovascular Research (DZHK), partner site Berlin, Berlin, Germany
[22]Institut für Laboratoriumsmedizin, University Hospital, LMU Munich, Munich, Germany
[23]Department of Dermatology, Allergy, and Venereology, University of Lübeck, Lübeck, Germany
[24]Department of Otorhinolaryngology, Technische Universität München and Klinikum Rechts der Isar, Munich, Germany
[25]These authors contributed equally
[26]Senior author
[27]Lead contact
*Correspondence: konstantin.stark@med.uni-muenchen.de (K.S.), admar.verschoor@tum.de (A.V.)
https://doi.org/10.1016/j.immuni.2024.08.007

SUMMARY

Venous thromboembolism (VTE) is a common, deadly disease with an increasing incidence despite preventive efforts. Clinical observations have associated elevated antibody concentrations or antibody-based therapies with thrombotic events. However, how antibodies contribute to thrombosis is unknown. Here, we show that reduced blood flow enabled immunoglobulin M (IgM) to bind to FcμR and the polymeric immunoglobulin receptor (pIgR), initiating endothelial activation and platelet recruitment. Subsequently, the procoagulant surface of activated platelets accommodated antigen- and FcγR-independent IgG deposition. This leads to classical complement activation, setting in motion a prothrombotic *vicious circle*. Key elements of this mechanism were present in humans in the setting of venous stasis as well as in the dysregulated immunothrombosis of COVID-19. This antibody-driven thrombosis can be prevented by pharmacologically targeting complement. Hence, our results uncover antibodies as previously unrecognized central regulators of thrombosis. These findings carry relevance for therapeutic application of antibodies and open innovative avenues to target thrombosis without compromising hemostasis.

INTRODUCTION

Antibodies (Abs) constitute a major component of humoral host defense, and they facilitate homeostatic clearance of altered or aged cells.[1] In addition, Abs are used therapeutically for the treatment of malignant and inflammatory diseases.[2] Several clinical lines of evidence suggest that Abs, irrespective of their source (endogenous/exogenous) or specificity (polyclonal/antigen specific), contribute to thrombosis: Ab therapies, ranging from anti-thymocyte globulin to anti-epidermal growth factor receptor (EGFR), anti-vascular epidermal growth factor receptor (VEGFR), or intravenous immunoglobulin (IVIG),[3] have been associated with a hypercoagulable state and thrombotic complications. Whether these findings relate to the specific mode of action of the Abs (i.e., their antigen specificity) or if Abs per se are prothrombotic is unclear.[4–15] Not only infusions with exogenous therapeutic Abs but also dysregulated production of endogenous Abs is linked to increased thrombosis risk, as in recently reported cases of vaccine-induced immune thrombotic thrombocytopenia, heparin-induced thrombocytopenia (HIT), antiphospholipid syndrome, multiple myeloma, or monoclonal gammopathy of undetermined significance.[16–20] Also here, the underlying mechanisms of the prothrombotic effects of such endogenous Abs remain unclear, as not all of these Abs appear to be linked to a targeted antigen.

Similar to Abs, the complement system—a main effector arm of Abs—has also been linked to thrombosis: elevated complement C3 concentrations in the normal population are associated with an increased risk of venous thromboembolism (VTE).[21] In infectious diseases, including COVID-19, complement correlates to a high risk for thrombotic events.[22–24] In addition, complement activation is associated with a prothrombotic state in thrombotic thrombocytopenic purpura.[25] In patients with systemic lupus erythematosus or primary autoimmune hemolytic anemia, generalized auto-Ab-driven complement activation is associated with a high risk of deep venous thrombosis (DVT) and deposition of complement factors on platelets.[26,27] Apart from Ab-triggered complement activation, increased Ab-independent complement activation is also associated with a prothrombotic state: genetic mutations in complement regulatory proteins in paroxysmal nocturnal hemoglobinuria (CD55 and CD59) or atypical hemolytic-uremic syndrome (e.g., factor H) are associated with thrombosis. Pharmaceutical complement targeting in these diseases also dampens their thrombotic risk.[28–31]

Here, we uncover how Abs and complement act together as central mediators of thrombosis *in vivo*. We show that the contribution of Abs is independent from their antigen-binding function and occurs in two phases, each dominated by distinct classes of Abs. First, flow reduction during DVT allows immunoglobulin M (IgM) to bind to endothelial cells (ECs), resulting in endothelial activation through FcμR (Toso) and the polymeric immunoglobulin receptor (pIgR). This initiates platelet and leukocyte recruitment through endothelial exposure of von Willebrand factor (vWF) and P-selectin. Second, the endothelial confined initiation process is followed by platelet activation, providing a procoagulant surface that promotes fibrin-dependent and chondroitin sulfate-A (CS-A)-dependent deposition of IgG, irrespective of Ab-antigen specificities or involvement of Fcγ receptors. These events initiate a complement-driven vicious circle of platelet activation and myeloid leukocyte recruitment that ultimately propagates clot formation. Together, our findings reveal an Ab-driven pathway that promotes thrombosis through the IgM receptors FcμR and pIgR, followed by IgG-mediated complement activation. We show that targeting this prothrombotic axis presents an innovative preventive and therapeutic option for thrombosis, one that, importantly, circumvents bleeding risks associated with conventional anticoagulation therapies.

RESULTS

Abs drive thrombosis through a bi-phasic mechanism

We tested the contribution of Abs to thrombosis in a mouse model of inferior vena cava (IVC) stenosis. While the thrombosis incidence of wild-type (WT) mice was within the expected range (>50%–60%) of the model,[32] animals lacking all secreted Abs (*Aicda*$^{-/-}$*Ighm*^{tm1Che}, also known as *AID*$^{-/-}$*sIgM*$^{-/}$) were strongly protected from thrombosis (Figure 1A). Ab deficiency also protected mice in a model of microvascular thrombosis (Figure S1A). DVT protection was lost when *Aicda*$^{-/-}$*Ighm*^{tm1Che} mice were reconstituted with polyclonal Ab-containing WT serum (Figure 1A). The DVT-protective phenotype was partially preserved in mice with isolated deficiency in secreted IgM (*Ighm*^{tm1Che}) but not in *Aicda*$^{-/-}$ mice that overproduce IgM but lack all other Ab isotypes, including IgG (Figures 1B and S1B). While circulating leukocyte or platelet counts could not explain the strain-specific differences in DVT susceptibility (data not shown), platelet recruitment to the endothelium within the first 3 h after inducing IVC stenosis (*initiating phase*) was attenuated in *Aicda*$^{-/-}$*Ighm*^{tm1Che} and *Ighm*^{tm1Che} mice, indicating a dominant role for IgM in local thrombosis initiation (Figure 1C). Moreover, IgM was consumed during DVT, and its baseline serum concentration correlated positively with thrombus weight (Figures S1C and S1D). IgM-sufficient *Aicda*$^{-/-}$ mice exhibited normal initial platelet recruitment, yet their deficiency in IgG hindered subsequent accumulation of platelets beyond 4 h of IVC stenosis (*propagation phase*) (Figures 1C and S1E). Consistent with a dominant role for IgG in thrombus propagation, loss of IgG—but not IgM—disturbed platelet aggregation and degranulation (Figure S1F). Nonetheless, neither deficiency in IgM nor IgG impaired coagulation *in vitro* or hemostasis *in vivo* (Figure 1D; data not shown).

The IgM-FcμR-pIgR axis initiates DVT

Since the clear prothrombotic activity of IgM could not be explained by a direct impact on platelets or coagulation, we investigated its prothrombotic contribution in more detail. Reconstitution of Ab-deficient *Aicda*$^{-/-}$*Ighm*^{tm1Che} mice with polyclonal IgM from naive WT mice restored thrombosis initiation as effectively as monoclonal IgM that was raised against the non-murine and thrombosis-irrelevant exogenous antigen keyhole limpet hemocyanin (Figures 1E and S1G). This indicates that specific antigen recognition by IgM is not relevant for its prothrombotic activity. IgM is a potent activator of the classical complement pathway (CP). Yet *Cμ13* mice—which express IgM that cannot bind C1q to activate the CP—showed normal thrombosis and platelet function (data not shown).

We next assessed a potential relevance of IgM receptors for the prothrombotic activity of IgM. Mice lacking FcμR (*Fcmr*$^{-/-}$)

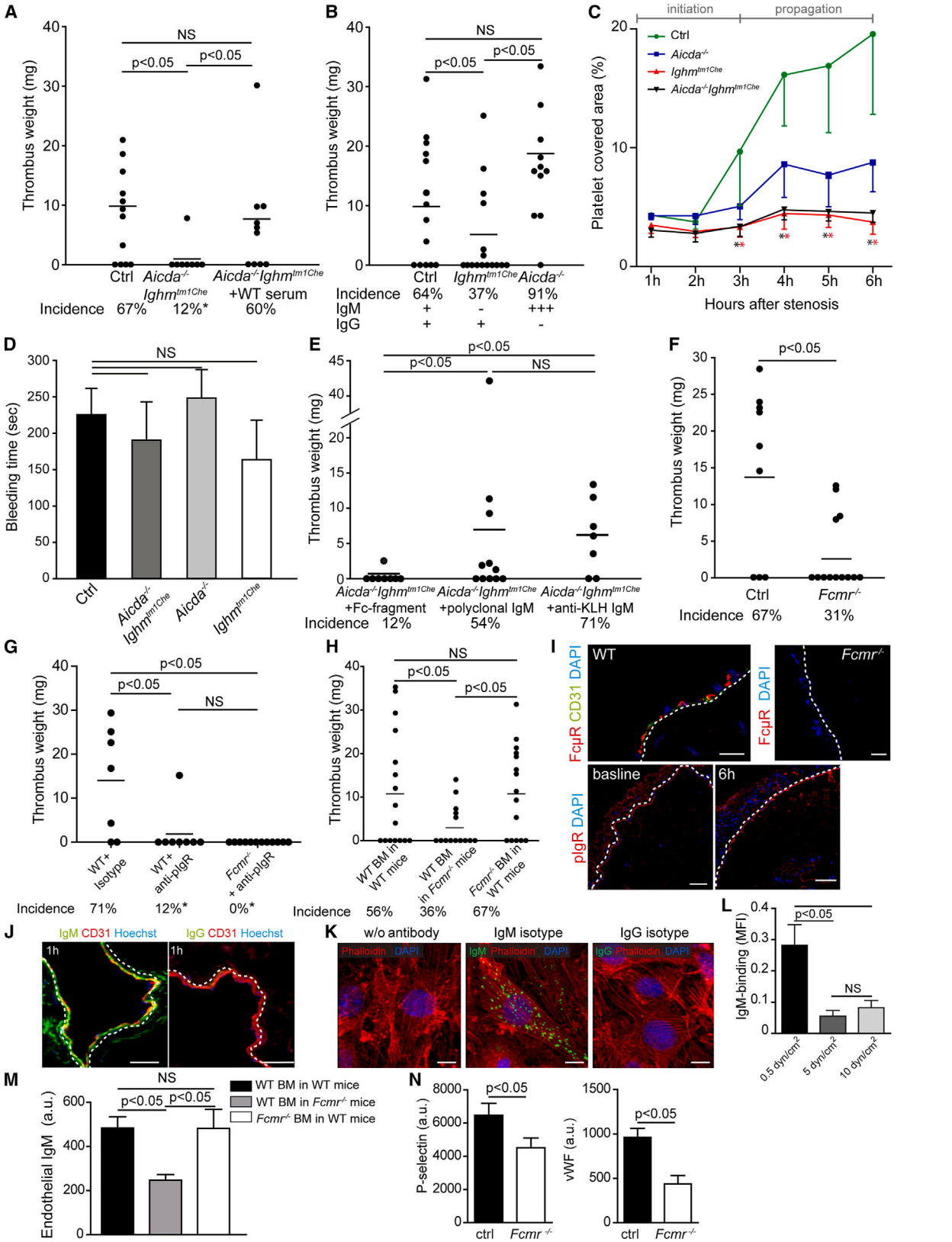

(legend on next page)

showed reduced thrombosis while retaining normal hemostasis, mirroring the reduced platelet recruitment of *Ighm*^{tm1Ch} mice over the first 6 h following flow reduction (Figures 1C, 1F, and S1H; data not shown). *Fcmr* deficiency combined with inhibition of pIgR, another IgM receptor expressed by ECs, completed the thromboprotective effect (Figure 1G).[33] The fact that combined ablation of FcμR and pIgR led to stronger thrombosis protection than ablation of their IgM ligand can be explained by the fact that complexed IgG1—shown in various studies to share functional properties with IgM pentamers[34,35]—also restored thrombus formation in *Ighm*^{tm1Che} mice and interacted with FcμR *in vitro*, while non-complexed IgG1 did not (Figures S1I and S1J). Although B cells express high amounts of FcμR,[36] our bone marrow chimeras suggested that non-hematopoietic FcμR is relevant for DVT development (Figure 1H). We found FcμR to be constitutively expressed on murine venous ECs (MVECs) and untreated IVCs isolated from WT mice *in vitro* under static conditions (Figure 1I). FcμR expression remained intact in IVCs from *Rag1*$^{-/-}$ mice that lack all B cells, further supporting that B cells do not contribute to vascular FcμR in the setting of DVT (Figure S1K). Moreover, we generated endothelial-specific FcμR deficient *VeCdhCreFcmr*$^{fl/fl}$ mice to address the contribution of endothelial FcμR to DVT. Although Cre recombinase-penetrance within the venous endothelium was variable, FcμR expression within the IVC correlated with thrombus weight in *VeCdhCreFcmr*$^{fl/fl}$ mice. Moreover, *VeCdhCreFcmr*$^{fl/fl}$ mice showed a further reduction in thrombosis when pIgR was additionally blocked (Figure S1L).[37,38] We found pIgR to be present *in vivo* on the IVC endothelium before as well as after flow reduction, while *in vitro* MVECs only expressed it under flow but not under static conditions (Figures 1I and S1M). FcαμR, a potentially third IgM receptor, was not detected in MVECs (Figure S1M). In line with the IgM-FcμR-pIgR axis initiating thrombosis, strong IgM deposition—but not IgG or IgA—was detected on IVC endothelium within 1 h of flow reduction (Figure 1J; data not shown). Also *in vitro*, deposition of IgM but not IgG was confirmed on MVECs: IgM bound to ECs under low-flow conditions that resemble reduced flow in IVC stenosis but not under normal venous flow conditions (Figures 1K, 1L, and S1N–S1P). In contrast, endothelial FcμR was present irrespective of flow conditions, pointing to flow reduction as decisive trigger enabling IgM-FcμR interaction on ECs (data not shown). The endothelial glycocalyx did not noticeably contribute to endothelial IgM deposition, while combined ablation of FcμR and pIgR was sufficient to reduce endothelial IgM signal to the same degree as IgM deficient mice (Figures 1M and S2A–S2D; data not shown).

Binding of IgM to endothelial IgM receptors FcμR and pIgR had remarkable functional consequences: ECs increased their adhesive properties for platelet GPIb and leukocyte PSGL-1 by exposing vWF and P-selectin in response to IgM but not IgG (Figure S2E). Consistently, upon stenosis, endothelial vWF exposure and P-selectin exposure were markedly decreased in *Fcmr*$^{-/-}$, compared with WT mice, and the additional pIgR blockade further reduced P-selectin but not vWF exposure (Figures 1N and S2F–S2H; data not shown). In *Fcmr*$^{-/-}$ mice, this translated into decreased platelet (Figure S1H) and leukocyte recruitment *in vivo* (Figure S2I). Thus, the prothrombotic effects of IgM are

Figure 1. IgM-FcμR interactions initiate venous thrombosis

(A) Thrombus weight and incidence in *Aicda*$^{+/+}$*Cμ*$^{+/+}$ mice (ctrl, $n = 12$), *Aicda*$^{-/-}$ *Ighm*^{tm1Che} ($n = 8$), and *Aicda*$^{-/-}$ *Ighm*^{tm1Che} mice supplemented with WT serum ($n = 10$), compared by one-way ANOVA followed by least significant difference (LSD) post hoc test or Fisher's exact test; * indicates $p < 0.05$ for incidence (Fisher's exact test). Line indicates mean.

(B) Thrombus weight and incidence in *Aicda*$^{+/+}$*Cμ*$^{+/+}$ mice (ctrl, $n = 14$), *Ighm*^{tm1Che} ($n = 16$), and *Aicda*$^{-/-}$ mice ($n = 11$), compared by one-way ANOVA followed by LSD post hoc test or Fisher's exact test. Line indicates mean.

(C) Quantification of platelet recruitment over the first 6 h after flow reduction in *Aicda*$^{-/-}$ *Ighm*^{tm1Che}, *Aicd*$^{+/+}$ *Ighm*^{tm1Che} ($n = 6$ each) compared with ctrl mice ($n = 13$) by one-way ANOVA followed by Tukey's multiple comparison test for each time point. * indicates $p < 0.05$ in the color of the respective group. See also Figure S1E.

(D) Tail bleeding time of C57BL/6 mice (ctrl, $n = 5$), *Ighm*^{tm1Che} ($n = 4$), *Aicda*$^{-/-}$ ($n = 4$), and *Aicda*$^{-/-}$ *Ighm*^{tm1Che} ($n = 4$) mice, compared by one-way ANOVA followed by Tukey's multiple comparison test.

(E) Thrombus weight and incidence in *Aicda*$^{-/-}$ *Ighm*^{tm1Che} receiving Fc-fragment ($n = 8$), pooled polyclonal IgM ($n = 11$), or anti-keyhole limpet hemocyanin (KLH) IgM ($n = 7$), compared by one-way ANOVA followed by LSD post hoc test or Fisher's exact test.

(F) Thrombus weight and incidence in C57BL/6 mice (ctrl, $n = 9$) compared with *Fcmr*$^{-/-}$ mice ($n = 10$) by two-tailed unpaired two-sample t test or Fisher's exact test. Line indicates mean.

(G) Thrombus weight and incidence in C57BL/6 mice treated with isotype ($n = 7$) or pIgR-blocking antibody ($n = 8$) and *Fcmr*$^{-/-}$ mice treated with pIgR-blocking antibody ($n = 12$), compared by one-way ANOVA followed by Tukey's multiple comparison test or Fisher's exact test. Line indicates mean.

(H) Thrombus weight and incidence in bone marrow chimeras: WT bone marrow into WT mice ($n = 16$), WT bone marrow into *Fcmr*$^{-/-}$ mice ($n = 15$), or *Fcmr*$^{-/-}$ bone marrow into WT mice ($n = 14$), compared by one-way ANOVA followed by LSD post hoc test or Fisher's exact test. Line indicates mean.

(I) Top: immunofluorescence staining for FcμR (red) and CD31 (green) in a cross-section of the IVC of C57BL/6 and *Fcmr*$^{-/-}$ mice under baseline conditions without manipulation of the IVC. Scale bar, 25 μm. Bottom: immunofluorescence staining for pIgR (red) in a cross-section of the IVC of C57BL/6 mice at baseline and 6 h after flow reduction. Scale bar, 50 μm; nuclei are stained with DAPI (blue). Dotted line indicates endothelium. Images representative of $n = 3$ experiments.

(J) Immunofluorescence staining for IgM (left, green) or IgG (right, green) and CD31 (red) of cross-section of the IVC 1 h after flow reduction in C57BL/6 mice. Nuclei are stained with Hoechst (blue). Dotted line indicating endothelium. Scale bar, 50 μm. Images representative of $n = 5$ experiments.

(K) Immunofluorescence staining of resting MVECs *in vitro* for phalloidin (red), DAPI (blue) after exposure to FITC-labeled isotype IgG1, or IgM (green) or PBS. Scale bar, 5 μm. Images representative of $n = 4$ experiments.

(L) Quantification of FITC-labeled isotype IgM binding to MVECs exposed to different shear stress (0.5, 5, and 10 dyn/cm^2) *in vitro* ($n = 7$–12 each). Data compared by one-way ANOVA followed by LSD post hoc test. See also Figures S1O and S1P.

(M) Quantification of endothelial IgM by immunofluorescence staining of cross-sections of the IVC 48 h after flow reduction compared by one-way ANOVA followed by Tukey's multiple comparison test. Left, bone marrow chimeras: WT bone marrow into WT mice, WT bone marrow into *Fcmr*$^{-/-}$ mice, *Fcmr*$^{-/-}$ bone marrow into WT mice ($n = 6$ each).

(N) Quantification of P-selectin and vWF exposure on the IVC in response to 6 h flow reduction in *Fcmr*$^{-/-}$ mice compared with control mice ($n = 5$ each), compared by two-tailed unpaired two-sample t test. (C, D, G, and L–N.) Data are shown as mean ± SEM.

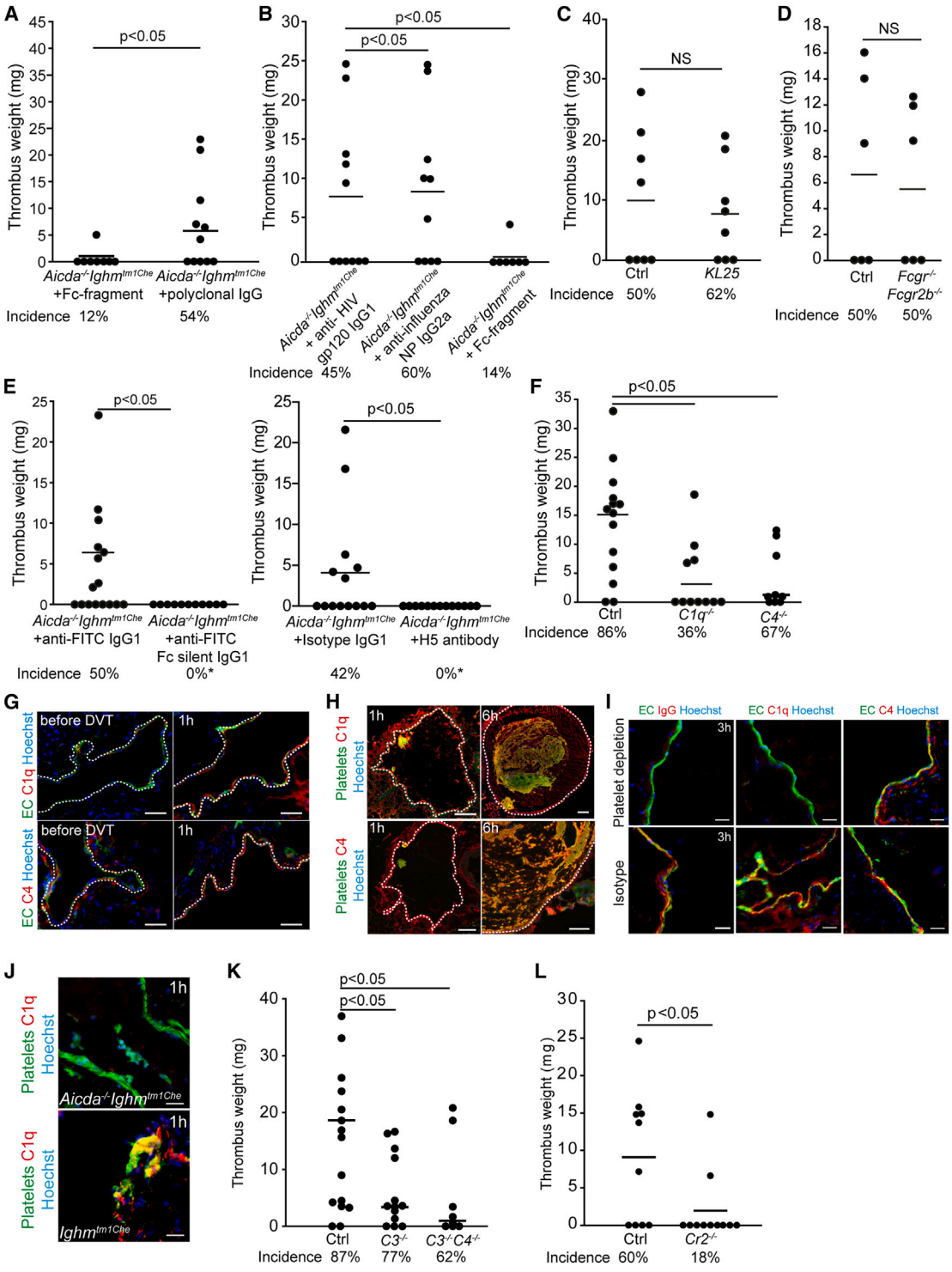

Figure 2. The prothrombotic effects of antibodies are independent from antigen binding and mediated by complement activation

(A–F) Thrombus weight and incidence in the IVC stenosis model. Line indicates mean.

(A) *Aicda*$^{-/-}$*Ighm*^{tm1Che} receiving Fc-fragment (n = 8) or pooled polyclonal IgG (n = 11), compared by two-tailed unpaired two-sample t test or Fisher's exact test.

(B) *Aicda*$^{-/-}$*Ighm*^{tm1Che} receiving anti-HIV gp120 IgG1 (n = 11), Fc-fragment (n = 7), or anti-influenza nucleoprotein (NP)2 IgG2a (n = 10), compared by one-way ANOVA followed by LSD post hoc test or Fisher's exact test.

(C) C57BL/6 mice (ctrl, n = 8) and *KL25* with normalized antibody concentrations (n = 8), compared by two-tailed unpaired two-sample t test or Fisher's exact test.

(D) C57BL/6 mice (ctrl, n = 6) compared with *Fcgr*$^{-/-}$*Fcgr2b*$^{-/-}$ mice (n = 6) by two-tailed unpaired two-sample t test or Fisher's exact test.

(legend continued on next page)

mediated through its interaction with FcμR and pIgR at reduced venous flow rates, increasing the adhesive properties of the endothelium for leukocytes and platelets.

IgG propagates thrombosis by classical CP activation

While Ab-deficient *Aicda*$^{-/-}$*Ighm*^{tm1Che} mice were fully protected from DVT, *Ighm*^{tm1Che} mutants lacking IgM but not IgG still formed small thrombi, indicating that class-switched Abs can be thrombogenic on their own, albeit less effectively (Figures 1A and 1B). Indeed, transfer of pooled polyclonal IgG restored thrombus formation in *Aicda*$^{-/-}$ *Ighm*^{tm1Che} mice (Figure 2A). In addition, polyclonal IgG supplementation to supraphysiologic concentrations further increased thrombus formation in WT mice (Figure S3A). This prothrombotic effect of IgGs was independent from IgG receptors, as mice lacking all known classical IgG-specific Fcγ receptors (*Fcgr*$^{-/-}$*Fcgr2b*$^{-/}$) showed normal DVT (Figure 2D). Furthermore, neither IgG sub-class (IgG1 or IgG2a isotypes) nor IgG antigen specificity (gp120 and NP viral antigens are non-murine and DVT irrelevant) were decisive factors in the ability of IgG to restore thrombus formation in Ab-deficient mice, while isolated IgG Fc-fragments proved insufficient (Figure 2B). The remarkable notion that the mere presence of IgG isotypes, irrespective of their antigen specificity, suffices to promote thrombosis was further supported by genetically targeted KL25 mice, which develop normal DVT, despite the fact that all their Abs are specific for the foreign, non-murine, DVT-irrelevant lymphocytic choriomeningitis virus (LCMV) glycoprotein (Figures 2C and S3B).[39] In contrast, *Aicda*$^{-/-}$ *Ighm*^{tm1Che} mice receiving a so-called "Fc-silent" derivative of a monoclonal IgG1 Ab – directed against the DVT-irrelevant, exogenous fluorescein isothiocyanate (FITC) antigen but unable to initiate the classical CP – did not develop DVT, whereas the complement-competent variant of the same clone was able to provoke thrombosis (Figure 2E). This finding was reproduced with another non-complement-activating IgG1 Ab, this time directed against trinitrophenol (TNP) as an irrelevant antigen, which also failed to induce thrombosis (Figure 2E) (Figure S3C).[40–43] In line with CP involvement, mice with targeted deficiencies in CP initiation (*C1q*$^{-/-}$) or CP propagation (*C4*$^{-/-}$ or *C3*$^{-/-}$) showed decreased DVT propagation, as reflected by unchanged incidence but decreased thrombus weight, while absence of key components in the mannose-binding lectin (MBL) or alternative pathway (factor B) did not protect from thrombosis (Figures 2F, 2K, and S2C). C4 was detectable within the endothelium before DVT onset, then co-localized with platelets and C1q on the endothelium within the first hours of flow reduction (Figures 2G and 2H). The luminal deposition of C1q and C4 required the presence of platelets and IgG (Figures 2I and 2J). CP activation generated both C4- and C3-derived opsonins, whose dual deficiency in *C3*$^{-/-}$*C4*$^{-/-}$ mice protected from thrombosis (Figure 2K). This protective phenotype was mirrored by *Cr2*$^{-/-}$ mice that lack binding of C3- and C4-derived opsonins by complement receptors 1 and 2 (CR1 and CR2) (Figure 2L), while mice with narrower deficits in binding C3-derived opsonin iC3b by CR3 and CR4 or C3-derived anaphylatoxin C3a by C3aR showed no decrease in thrombus formation (Figures S3D and S3E). Moreover, neither the terminal pathway (*C5*$^{-/-}$) nor C5aR appeared to have a major contribution to thrombus formation (Figure S3F). Accordingly, while C5 deficiency had no effect, *Cr2*$^{-/-}$ and *C3*$^{-/-}$*C4*$^{-/-}$ strains showed clear neutrophil recruitment deficits to the growing thrombus, and absence of C1q, C3, or C4 impaired prothrombotic neutrophil extracellular trap formation (NETosis) (Figures S3G–S3I).[44–46] Thus, IgG promotes thrombus propagation independent from its antigen specificity by fostering a prothrombotic innate immune cycle involving CP complement activation, neutrophil recruitment, and NETosis.

IgG locates to the thrombogenic platelet surface

For polyclonal IgG to exert its prothrombotic effect in Ab-deficient mice, the presence of platelets was essential (Figure 3A). While IgM primarily deposited along the endothelium during DVT, IgG localized to platelets within the thrombus itself in an antigen-independent manner (Figures 3B and S4A). Non-specific IgG1 associated with activated but not with resting platelets *in vitro* (Figures 3C and 3D). Activation changed the platelet surface, exposing CS-A and activating fibrin(-ogen) receptor GPIIb/IIIa.[47,48] Blockade of GPIIb/IIIa with tirofiban not only prevented activated platelets from binding fibrin(-ogen), but it simultaneously abrogated their association with IgG (Figures 3E and S4B). We found that IgG adsorbed well to deposited fibrin, especially in the presence of CS-A, and consequently, degradation of CS-A from activated platelets decreased IgG deposition (Figures S4C and S4D). The presence of activated platelets improved IgG deposition on fibrin—but not on fibrinogen—*in vitro* (Figure 3F). In contrast, albumin, an abundant plasma protein with intrinsic platelet-binding properties, neither affected platelet-IgG interactions nor thrombus formation (data not shown).[49] IgG deposition on activated human platelets was independent from platelet FcγRIIA, and the transgenic expression of *Fcgr2a* on murine platelets neither affected DVT *in vivo* nor the

(E) *Aicda*$^{-/-}$ *Ighm*^{tm1Che} receiving anti-FITC IgG1 (n = 16) compared with anti-FITC Fc-silent IgG1 (n = 11) by two-tailed unpaired two-sample t test or Fisher's exact test.
(F) C57BL/6 (ctrl, n = 14), *C1q*$^{-/-}$ (n = 11), or *C4*$^{-/-}$ mice (n = 9), compared by one-way ANOVA followed by LSD post hoc test or Fisher's exact test.
(G) Immunofluorescence staining of the IVC before and 1 h after flow reduction for C1q (red, top) or C4 (red, bottom) and endothelial cells (ECs, CD54, green); nuclei stained by Hoechst (blue). Dotted line indicates endothelium. Scale bar, 40 μm. Images representative of n = 4 experiments.
(H) Immunofluorescence staining of the IVC 1 and 6 h after flow reduction for C1q (red, top) or C4 (red, bottom) and platelets (CD42b, green); nuclei stained by Hoechst (blue). Dotted line indicates endothelium. Scale bar, 100 μm. Images representative of n = 5 experiments.
(I) Immunofluorescence of the vessel wall of the IVC 3 h after flow reduction stained for endothelial cells (ECs, CD54, green), IgG (red, left), C1q (red, middle), C4 (red, right), or/and Hoechst (blue) in C57CL/6 mice after platelet depletion or isotype control antibody application. Images representative of n = 5 experiments.
(J) Immunofluorescence of the vessel wall of the IVC 1 h after flow reduction stained for platelets (CD42b, green), C1q (red), and Hoechst (blue) in *Aicda*$^{-/-}$*Ighm*^{tm1Che} (top) and *Ighm*^{tm1Che} (bottom) mice. Scale bar, 40 μm. Representative of n = 5 experiments. Scale bar, 30 μm. Representative of n = 5 experiments.
(K) C57BL/6 (ctrl, n = 15) compared with *C3*$^{-/-}$ (n = 13) and *C3*$^{-/-}$*C4*$^{-/-}$ mice (n = 8), compared by one-way ANOVA followed by LSD post hoc test or Fisher's exact test.
(L) C57BL/6 (ctrl, n = 10) compared with *Cr2*$^{-/-}$ mice (n = 11) by two-tailed unpaired two-sample t test or Fisher's exact test.

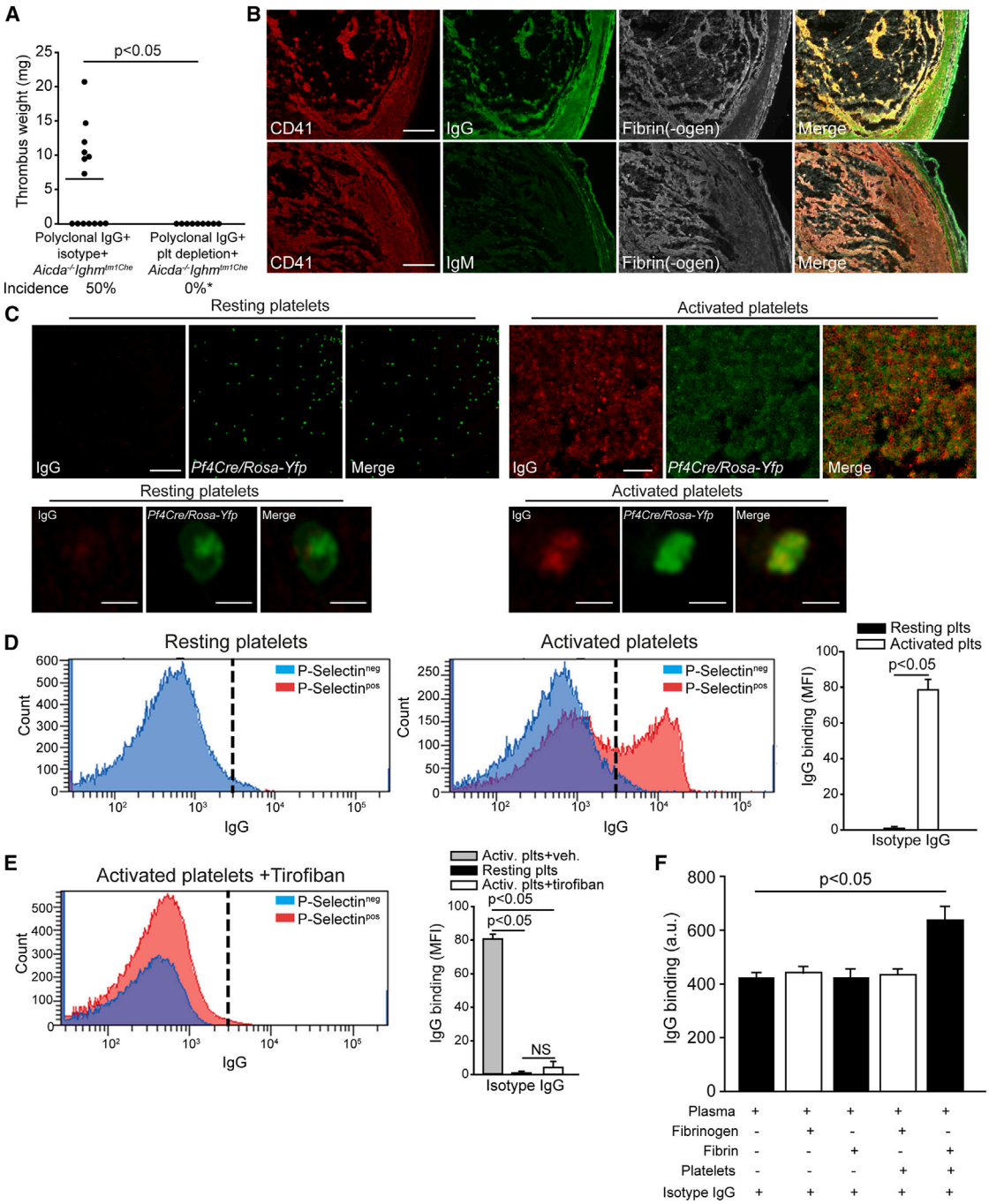

Figure 3. Activated platelets serve as a platform for antibody deposition and complement activation

(A) Thrombus weight and incidence in *Aicda*$^{-/-}$*Ighm*^{tm1Che} mice receiving pooled polyclonal IgG together with platelet depletion (n = 14) or isotype antibody control (ctrl, n = 9), compared by two-tailed unpaired two-sample t test or Fisher's exact test. Line indicates mean.

(B) Immunofluorescence staining of cross-sections of the IVC 48 h after flow reduction from C57BL/6 mice for CD41 (red), IgG (top) or IgM (bottom) in green, and fibrin(-ogen) (gray). Scale bar, 75 μm. Representative of n = 4 experiments.

(C) Representative images of washed platelets from *Pf4Cre*$^{+}$*Rosa-Yfp* mice (green) *in vitro*. Top: binding of isotype IgG1 (red) to PAR4 agonist activated (right) but not resting platelets (left). Scale bar, 10 μm. Bottom: higher magnification of IgG binding to single platelets. Scale bar, 2 μm. Representative of n = 4 experiments.

(D) Flow cytometry analysis of isotype IgG1 binding to washed platelets, P-selectin^{pos} (red) or P-selectin^{neg} (blue) platelets. Left: flow cytometry analysis of isotype IgG1 binding to resting platelets; Middle: isotype IgG1 binding to PAR4 agonist activated platelets. Representative of n = 5 experiments. Right: quantification of isotype IgG1 binding to PAR4 agonist activated compared with resting platelets (n = 5 each).

(E) Left: flow cytometry analysis of isotype IgG1 binding to PAR4 agonist (thrombin receptor activating peptide [TRAP]) activated washed P-selectin^{+} (red) or P-selectin^{-} (blue) platelets incubated with tirofiban gated on platelet singlets. Representative of n = 4 experiments. Right: quantification of isotype IgG1

(legend continued on next page)

deposition of IgG onto platelets *in vitro* (Figures S4E–S4I). The previously observed platelet activation defects in platelet-rich plasma (PRP) from *Aicda*$^{-/-}$ *Ighm*^{tm1Che} mice could be rescued by supplementation with WT plasma, thus excluding platelet-intrinsic defects and rather pointing toward Ab contributions, possibly also IgG from intracellular platelet pools (Figure 4A). The activating effect of IgG was further supported by the finding that polyclonal IgG fostered platelet aggregation and ATP release in a dose-dependent manner in PRP from *Aicda*$^{-/-}$ *Ighm*^{tm1Che} mice (Figure 4B). This platelet-activating effect of IgG was antigen independent, as platelets in PRP from *KL25* mice or from Ab-deficient mice supplemented with anti-FITC IgG1—both settings where Abs are directed to non-murine, DVT-irrelevant antigens—still showed normal function (Figures 4C and 4D). In contrast, a non-C1q-binding variant of the same anti-FITC IgG1 clone failed to rescue platelet function (Figure 4D). The requirement for early complement activation was further confirmed in PRP from *C1q*$^{-/-}$ and *C3*$^{-/-}$ mice (Figure 4E).[50] In line, consumption of circulating platelets was reduced in *C1q*$^{-/-}$ and *C3*$^{-/-}$ mice, and recruitment of platelets to the thrombus core, especially in *C1q*$^{-/-}$ mice, was impaired (Figures 4F and 4G). Despite their thrombo-protective phenotype, *C1q*$^{-/-}$, *C3*$^{-/-}$, and *C4*$^{-/-}$ mice had normal coagulation, mirroring the phenotype previously observed in Ab-deficient mice (data not shown). Complement activation on platelets affects neutrophils.[51] Accordingly, stimulated platelets triggered NETosis in a C1q-, C3-, and C4-dependent and neutrophil CR2-dependent manner *in vitro*, with NETosis reduced in *Cr2*$^{-/-}$ mice *in vivo* (Figures S4J and S4K). Together, our data show that fibrin and CS-A, rather than Ab-antigen interactions or FcγRIIA, localize IgG to activated platelets in DVT, stimulating platelet activation and thrombus growth via CP complement activation.

Complement is a therapeutic target in DVT

To extend our murine findings to humans, we assessed human varicose veins and COVID-19 plasma/autopsy specimens. Not unlike our murine model of IVC stenosis, human varicose veins provide a unique opportunity to investigate veins that combine reduced blood flow with increased DVT risk.[52] Analogous to mice, pronounced endothelial IgM deposition was only detected in varicose veins, as well as human ECs held under low-flow conditions Moreover, while endothelial FcμR was detectable both on extracted healthy and varicose human veins, only varicose veins co-expressed pIgR (Figures 5A, 5B, and S5A). Moreover, we observed co-localization of IgG and C1q with platelet aggregates covering the endothelium of varicose—but not healthy—veins, accompanied by downstream CP C3 and C4 activation products (Figures 5C, S5B, and S5C). Similar to mice, IgG deposition on activated human platelets *in vitro* was prevented by blocking fibrin association with GPIIb/IIIa, using the antagonist tirofiban (Figures S5D and S5E). We further extended our human observations by examining pulmonary thrombi specimen from COVID-19 autopsy patients and identified the identical pattern of IgG and C4 deposition onto platelets, even though the initiation mechanism (infection) may have been different from DVT (flow reduction) (Figure 5D). As in mice, CP complement—but not the alternative, lectin, or terminal pathway—correlated with thrombosis (represented by elevated D-dimer concentrations) in hospitalized COVID-19 patients (Figures 5E and S5F). Given the fact that we found platelet-IgG-complement patterns to be preserved between human and mice, we tested whether IgG-dependent CP activation might be exploited therapeutically for DVT prevention. Our DVT experiments in mice with isolated C1q or C3 deficiencies already predicted that pharmacological targeting of either C1q or C3 alone might be insufficient to fully prevent thrombosis, while the more pronounced DVT reduction seen in *C3*$^{-/-}$*C4*$^{-/-}$ mice was suggestive of a synergistic effect for early and late CP factors (see Figure 2K; Figure 5F). In line with this, simultaneous but not singular targeting of C1q and C3, using cobra venom factor (CVF) or recombinant murine Crry protein, protects WT mice from thrombosis (Figure 5F). Importantly, and in line with our observations in genetically complement-deficient mice, simultaneous therapeutic targeting of C1q and C3 did not impair hemostasis (data not shown). Moreover, combined therapeutic targeting of C1q and C3 also led to reduced platelet deposition in the lungs of severe acute respiratory syndrome coronavirus 2 (SARS-CoV-2)-infected mice and prevented systemic platelet aggregation, while leaving NETosis unaffected (Figures 5G, S5G, and S5H; data not shown). We thus demonstrate that IgG-dependent complement activation not only can serve as a previously unknown but effective therapeutic pathway to prevent DVT, but it can be equally effective to control dysregulated immunothrombosis as it can occur in severe COVID-19. Importantly, this approach circumvents the bleeding risks associated with anticoagulants traditionally used in thrombosis therapy and prophylaxis (Figure S5I).

DISCUSSION

Our study has revealed a prothrombotic function of Abs that is independent from their specific antigen binding, and it establishes Abs and complement as key connectors at the interface between inflammation and thrombosis. Our findings have several important clinical implications: (1) we identified Ab-driven complement activation and IgM receptors as innovative targets for the treatment and prevention of DVT, which—unlike anticoagulation with its inherent bleeding risk—do not affect hemostasis; (2) we have provided detailed mechanistic insights into previously unexplained clinical observations linking diseases associated with excess Ab production to thrombotic events[18,19]; (3) our data has provided mechanistic information regarding the association of Ab therapeutics and thrombotic events and identified complement and platelets as potential targets to control these side effects[5,7,12–15,53,54]; and (4) we identified CP consumption—independent from downstream terminal pathway

binding to resting or PAR4 agonist (TRAP) activated platelets incubated with PBS (vehicle) or tirofiban (n = 4 each), compared by one-way ANOVA followed by LSD post hoc test. See also Figure S4B.

(F) Quantification of fluorescence intensity of isotype IgG1 binding to surfaces covered with plasma only, or plasma with addition of one or more of the following: fibrin, fibrinogen, or platelets (n = 4 each); conditions were compared by one-way ANOVA followed Tukey's multiple comparison test. (D–F) Data shown as mean ± SEM.

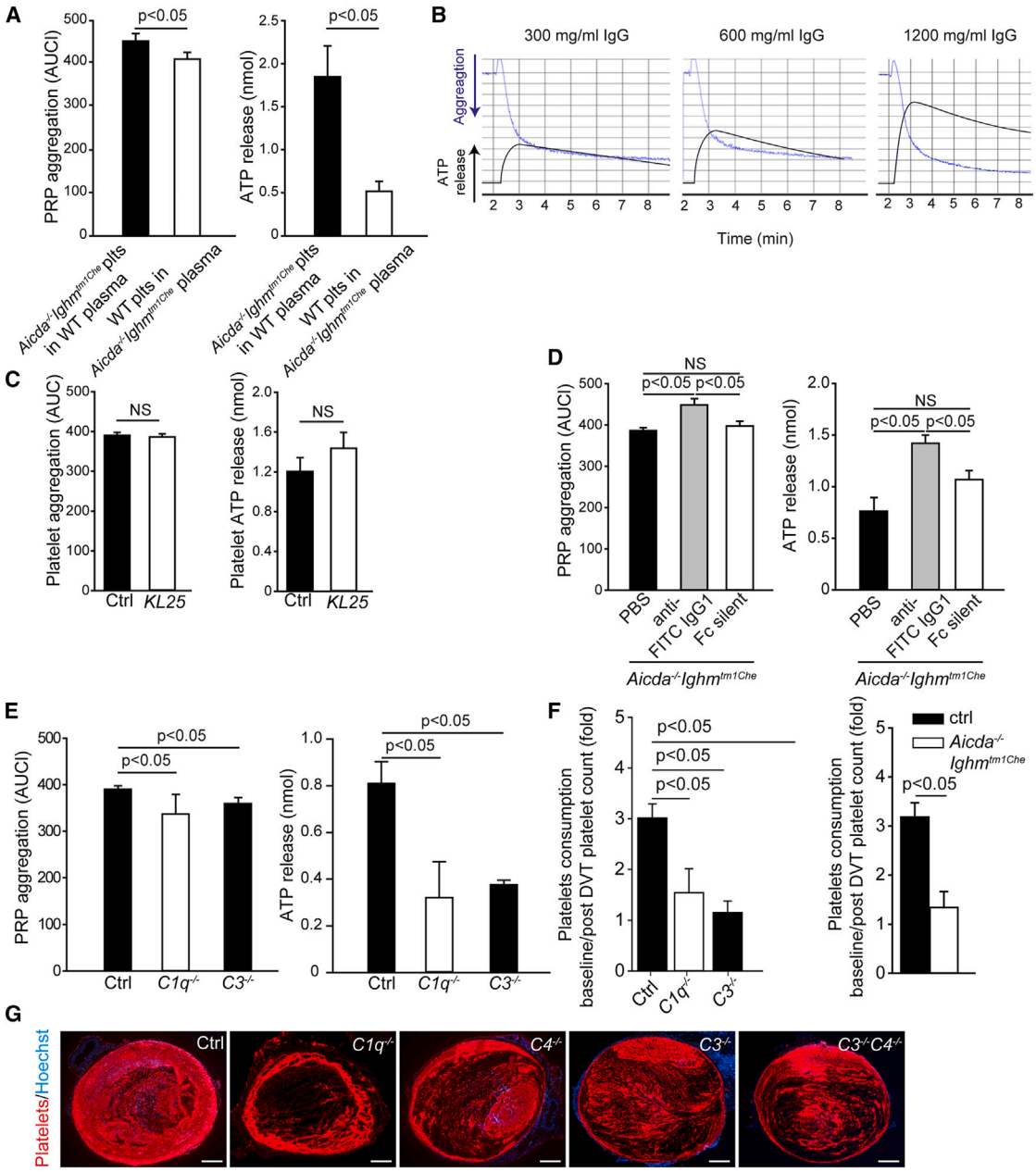

Figure 4. Antibody deposition on platelets triggers complement activation

(A) Aggregometry of washed platelets from *Aicda*$^{-/-}$*Ighm*^{tm1Che} (n = 5) mice and WT plasma or WT platelets with *Aicda*$^{-/-}$*Ighm*^{tm1Che} (n = 5) plasma showing platelet aggregation (left) and ATP release (right), compared by two-tailed unpaired two-sample t test.

(B) Representative examples of aggregometry of platelet-rich plasma from *Aicda*$^{-/-}$*Ighm*^{tm1Che} supplemented with different amounts of polyclonal IgG (n = 5 each) showing platelet aggregation (blue line starting from top) and ATP release (black colored line starting from bottom).

(C) Aggregometry of platelet-rich plasma from WT (n = 4) or *KL25* mice (n = 4) with normalized antibody concentrations showing platelet aggregation (left) and ATP release (right), compared by two-tailed unpaired two-sample t test.

(D) Aggregometry of platelet-rich plasma from *Aicda*$^{-/-}$*Ighm*^{tm1Che} (n = 5) mice with addition of PBS, anti-FITC IgG1, or anti-FITC IgG1 Fc silent showing platelet aggregation (left) and ATP release (right), compared by one-way ANOVA followed by LSD post hoc test.

(E) Aggregometry of platelet-rich plasma from ctrl, *C1q*$^{-/-}$, and *C3*$^{-/-}$ mice (n = 5 each) showing ATP release (right) and platelet aggregation (left), compared by one-way ANOVA followed by LSD post hoc test.

(F) Platelet consumption from C57BL/6 (ctrl), *C1q*$^{-/-}$, and *C3*$^{-/-}$ mice (n = 5 each), compared by one-way ANOVA followed by LSD post hoc test, or *Aicda*$^{+/+}$*C*$\mu^{+/+}$ (WT) and *Aicda*$^{-/-}$*Ighm*^{tm1Che} mice (n = 6 each) compared by unpaired t test.

(G) Immunofluorescence staining of cross-sections of the IVC 48 h after flow reduction for platelets (CD41, red) and Hoechst (blue) in *C1q*$^{-/-}$, *C4*$^{-/-}$, *C3*$^{-/-}$, *C3*$^{-/-}$*C4*$^{-/-}$, or ctrl mice. Scale bar, 100 μm. Representative of n = 3–5 experiments. (A and C–F) Data given as mean ± SEM.

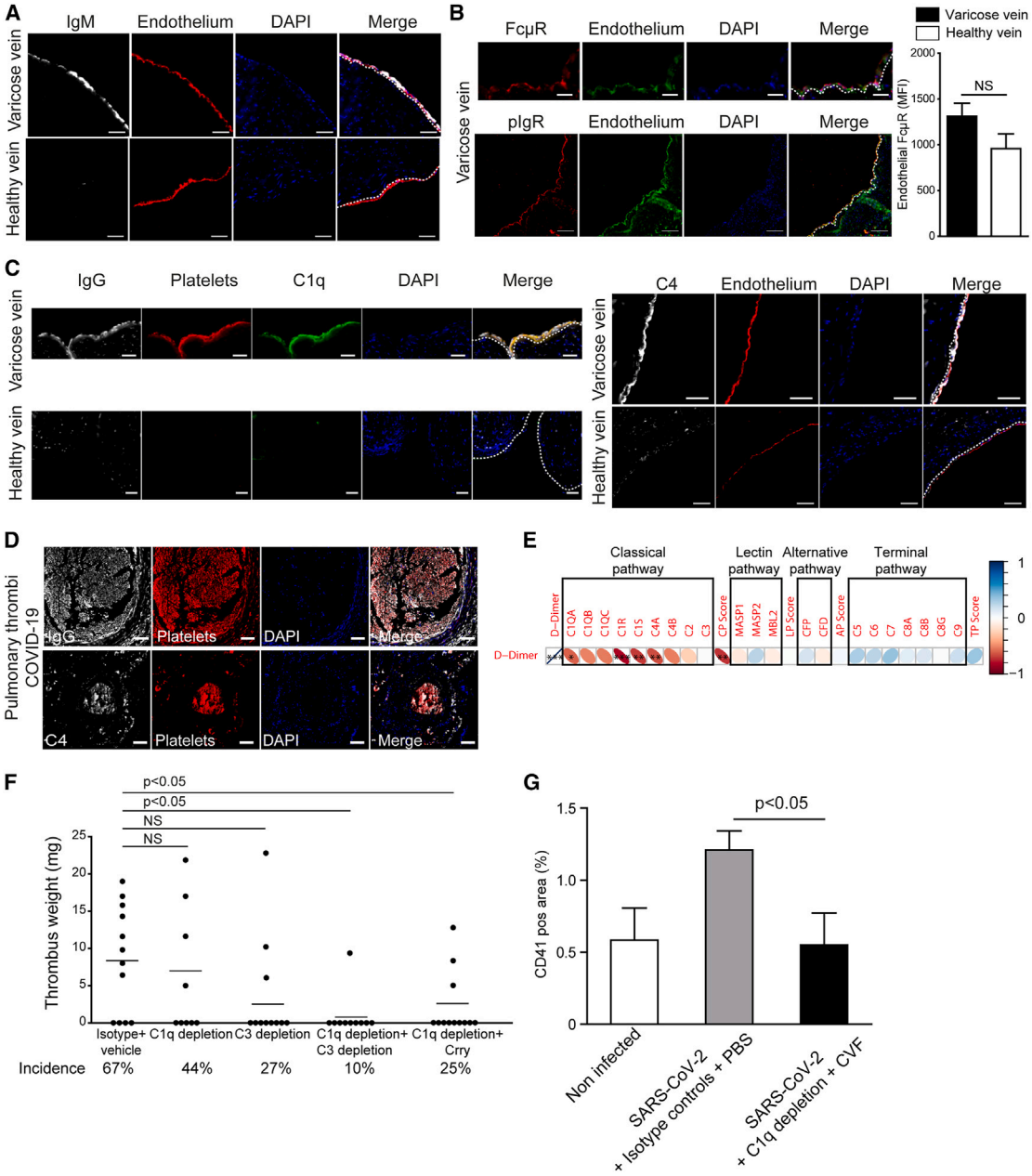

Figure 5. Complement activation triggered by platelet-antibody interaction as therapeutic target in DVT

(A–C) Immunofluorescence staining of human varicose veins (top) and healthy veins (bottom) for: (A) IgM (white) and endothelium (ICAM-1, red); scale bar, 50 μm. (B) Left top: FcμR (red) and endothelium (ICAM-1, green). Left bottom: pIgR (red) and endothelium (CD31, green). Scale bar, 20 μm; right: quantification of endothelial FcμR (n = 8 each) given as mean fluorescence intensity (MFI). Data given as mean ± SEM and compared by two-tailed unpaired two-sample t test. (C) Left: IgG (white), platelets (CD42b, red), and C1q (green). Scale bar, 30 μm; right: C4 (white) and endothelium (ICAM-1, red). See also Figures S5B and S5C. (A–C) Dotted line indicated endothelium, DAPI in blue. Representative of n = 8 independent samples each.

(D) Pulmonary autopsy specimens from COVID-19 patients. DAPI in blue. Representative of n = 6. Top: staining for platelets (CD42b, red) and IgG (white). Scale bar, 50 μm. Bottom: staining for platelets (CD42b, red) and C4 (white). Scale bar, 50 μm.

(E) Proteome analysis for the correlation of D-dimer and complement factors as well as activation pathways given as scores: classical pathway (CP), lectin pathway (LP), alternative pathway (AP), terminal pathway (TP). p values, indicating slope significantly non-zero, are displayed as $^{*}p < 0.05$, $^{**}p < 0.01$, and $^{***}p < 0.001$. Positive correlations are shown in blue and negative correlations in red. Color intensity and the size of the ellipse are proportional to the correlation coefficient. See also Figure S5F.

(F) Thrombus weight and incidence in C57BL/6 mice receiving isotype rat IgG1 and PBS (n = 12), C1q depletion (n = 9), C3 depletion (n = 11), C3/C1q depletion (n = 10), or C1q depletion combined with complement inhibitor Crry (n = 12), compared by one-way ANOVA followed by Tukey's multiple comparison test.

(G) Quantification of platelets from immunofluorescence staining of lungs from non-infected (n = 2) or SARS-CoV-2-infected mice with control or complement depletion treatment (n = 4 each). Data given as mean ± SEM and infected groups compared by two-tailed unpaired two-sample t test. See also Figures S5G and S5H.

activation—to correlate with coagulation and pulmonary thrombi in COVID-19 patients. Together with our findings in mice, this supports potential benefits of upstream CP complement therapeutics in relation to thrombotic complications in COVID-19.[55]

We have shown that DVT proceeds in two distinct Ab isotype-dependent phases. First, reduced blood flow velocity allowed IgM binding to the endothelium, activating it through FcμR and pIgR, which resulted in surface exposure of P-selectin and vWF, thereby initiating platelet recruitment to the veins.[46,56] Second, this IgM-driven "initiation phase" is followed by an IgG-driven "propagation phase," in which fibrin and CS-A on activated platelets enable IgG to deposit onto the platelet surface, triggering CP activation, thereby setting in motion a prothrombotic *vicious circle* of platelet and neutrophil activation. These prothrombotic effects of IgM and IgG can materialize at physiological Ab concentrations, excluding high "blood viscosity" associated with elevated Ab concentrations as an explanation.[57]

Interaction between IgM and endothelial FcμR only commences at low-flow rates, consistent with the reduced blood flow rates found in, for instance, varicose veins or venous stenosis/stasis. Continuous rebinding effects are especially relevant for low-affinity interactions like that between IgM and FcμR, so that reducing the flow rate increases ligand-receptor interactions. Therefore, reduced flow enables prolonged interaction of IgM and EC-expressed FcμR.[58,59] Moreover, our data implicate that IgG1 complexation—as opposed to IgG1monomers—may increase the FcμR-binding properties of IgG1, not unlike the IgM-like complement-activating properties IgGs were shown to gain upon hexamerization.[34,35] The fact that DVT was initiated by IgM interaction with FcμR and pIgR, irrespective of the IgM antigen specificity, argues against a role for natural IgM recognizing specific antigens associated with tissue stress or injury.[60,61] In fact, *Fcmr*$^{-/-}$ mice are protected from thrombosis despite their elevated concentrations of natural IgM.[62] Also, the elevated IgM concentrations of *Aicda*$^{-/-}$ mice did not further enhance platelet recruitment, possibly because physiological IgM concentrations were already sufficient to saturate IgM receptors. Besides FcμR, we found pIgR to be another endothelial IgM receptor contributing to the initiation of DVT in a flow-dependent manner. In contrast to FcμR, which drives venous endothelial P-selectin and vWF exposure upon interacting with IgM, we found regulation by pIgR to be limited to P-selectin.

The prothrombotic effect of IgG described here did not rely on antigen specificity, while antigen-dependent thrombosis—for instance in anti-phospholipid syndrome or HIT—is mediated by limited amounts of antigen-specific (auto)Abs with great prothrombotic potency.[63,64] Another key difference between our findings and an immune complex-driven prothrombotic disease like HIT is that heparin-Ab complexes activate platelets via FcγRIIA, a receptor not present on murine platelets.[16,65] Therefore, and although we find it to be preserved in humans too, the Ab-driven prothrombotic mechanism we uncover here can proceed in full independence of FcγRIIA. Rather than engaging FcγRIIA, IgG deposition on activated platelets in our setting relied on fibrin and CS-A, reminiscent of the reported CP-activating association of IgG with biomaterial surfaces, and is independent from platelet FcγRIIA.[66–69]

Closely related mechanisms, also involving Abs, complement, platelets, and fibrin, and collectively referred to as "immunothrombosis," regulate the systemic clearance and phagocytic removal of bacteria.[50,70–75] Our data in mice and humans implicate that overshooting activation of immunothrombosis in COVID-19 could involve Ab deposition and CP activation on platelets, contributing to the increased risk of thrombosis in SARS-CoV-2 infection, even though the initiation mechanisms may differ from the ones observed for flow reduction-induced DVT.[76–78] Although antigen-independent IgG localization does not follow "textbook" Ab-antigen binding rules, its prothrombotic properties rely on the ability to recruit C1q. C1q can also bind and activate platelets independent from its further downstream classical pathway activity,[79] providing an explanation for the observed synergistic contributions of C1q and C3 in DVT, beyond their expected sequential roles in the CP. In addition, the procoagulant surface of activated platelets fostered further complement activation and neutrophil recruitment in a C3- and C4-dependent and CR1- and/or CR2-dependent manner, while C5 had no detectable contribution. This is in line with a context-dependent prothrombotic effect of the terminal pathway, since C5 activation principally leads to a prothrombotic phenotype when it causes ADP release by cytolysis.[80] This notion is further supported by our finding that CP activation associated with elevated D-dimer concentrations in COVID-19 patients without observable terminal pathway involvement.

Our data reveal that, unlike coagulation, the complement system does not have a strong negative impact on hemostasis, so that targeting the Ab-complement axis governing DVT offers a way to uncouple thrombosis from hemostasis. So far, thrombosis treatment and prevention rely exclusively on anticoagulation with its inherent bleeding risks. A broad spectrum of highly specific complement therapeutics now offers alternatives.[81] Our identification of key molecular, histological, and pathological parallels between murine and human DVT motivated us to test the efficacy of such complement inhibitors in DVT. We show in mice that both complement depletion and complement regulation can provide effective strategies to prevent thrombosis. Given the reported impact of complement on general immune defenses and also bleeding, patients will need to be closely monitored in each particular clinical setting.[82] Nonetheless, complement inhibition strategies with only moderate impact on coagulation can provide promising alternatives for patients with simultaneous thrombotic and bleeding risks (i.e., surgery, intracranial hemorrhage, polytrauma).

Another important clinical implication of our study is that it provides a mechanistic explanation for recent reports that connect SARS-CoV-2 vaccination[17] and several Ab therapies—as recently shown for IVIG therapy in dermatomyositis[3]—with thrombotic events.[5,7,12–14,18,53,54] While antigen-specific interactions or FcγRIIA engagement can certainly contribute to the prothrombotic effects of a number Ab therapies, our data now provide an explanation for an antigen- and FcγRIIA-independent mechanism too. This dose-dependent prothrombotic mechanism is particularly relevant in the setting where high amounts of IVIG are administered. Consistent with our finding that activated platelets provide a platform for IgG-dependent complement activation, settings with general platelet activation form a risk factor for thrombosis in patients receiving IVIG. This increased risk of thrombosis could be reduced with platelet inhibition.[7,83,84]

In summary, besides providing fundamental insights into the pathophysiological mechanisms governing thrombosis, our findings also have broad clinical implications for the treatment and prevention of thrombosis, as well as for the development and application of therapeutic Abs.

Limitations of the study

In this study, we used mice to dissect roles for complement and Abs in thrombosis. Although our data show that important hallmarks are shared between human and murine thrombosis, we cannot rule out that mechanistic aspects may differ between species. We use a well-established murine DVT model, but we do not claim it to reflect the full pathophysiology of thrombosis in immobilized or aged humans.

In contrast to several published studies, our data strongly suggest a non-hematopoietic, endothelial source of FcμR. More detailed studies are welcomed to definitively prove whether the endothelium is indeed the definitive source of FcμR and pIgR responsible for mediating IgM interactions with the endothelium and for driving thrombosis.

Continual developments and refinements in (targeted) complement therapeutics offer perspectives for more fine-tuned interventions, beyond the experimental and indiscriminate depletion strategies we used here to principally showcase the value of complement as therapeutic target in venous thrombosis.

RESOURCE AVAILABILITY

Lead contact

Further information and requests for resources and reagents should be directed to and will be fulfilled by the lead contact, Konstantin Stark (konstantin.stark@med.uni-muenchen.de).

Materials availability

Materials are available upon request from the lead author.

Data and code availability

All data reported in this paper will be shared by the lead contact upon request. This paper does not report original codes. Any additional information required to reanalyze the data reported in this paper is available from the lead contact upon request.

ACKNOWLEDGMENTS

We thank Michael Carroll (Harvard Medical School, Boston) for providing *Ighm*^{tm1Che}, *C4*$^{-/-}$, and *C3*$^{-/-}$ mice; Mark Suter (University of Zurich, Zurich) for providing *Aicda*$^{-/-}$ mice; Marina Botto (Imperial College London, London) for providing *C1q*$^{-/-}$ and *fB*$^{-/-}$ mice; Craig Gerard (Harvard Medical School, Boston) for providing *C3aR*$^{-/-}$ mice; Falk Nimmerjahn (University Erlangen-Nuernberg, Erlangen) for providing *Fcgr*$^{-/-}$*Fcgr2b*$^{-/-}$ mice; Karl Lang (University of Duisburg-Essen, Essen) for providing *Fcmr*$^{-/-}$ mice; Hans Hengartner and Rolf Zinkernagel (ETH Zurich, Zurich) for providing *KL25* mice; Mark Zabel (University Hospital of Zurich, Zurich) for providing *CR2*$^{-/-}$ mice; Christie Ballantyne (Baylor College of Medicine, Houston) for providing *CD11c*$^{-/-}$ mice; and Siamon Gordon (University of Oxford, Oxford) for providing *CD11b*$^{-/-}$ mice. A.V. wishes to thank Michael Grünaug and dedicates this work to Annette, Rita, and Hans.

This project has received funding from the European Research Council (ERC) under the European Union's Horizon 2020 research and innovation programme (grant agreement no. 947611) (K.S.). This study was supported by the Deutsche Forschungsgemeinschaft through the collaborative research center 914 project B02 (K.S. and S.M.), project B04 (A.V.), project A01 (M.M.), project B01 (M.S.), the collaborative research center 1123 project B07 (K.S. and S.M.), the collaborative research center 359 (project A03 [K.S.] and B02 [M.S.]), the international research training group 1911 project B09 (A.V.), the clinical research unit 303 project 7 (A.V.), cluster of excellence 2167 (A.V.), collaborative research center 1526 project 05 (A.V.), the ANR-DFG project JAKPOT (K.S.), LMUexcellent (K.S.), and the Deutsche Zentrum für Herz-Kreislauf-Forschung (PostDoc Grant and partner site project [K.S. and S.M.]). M.I. is supported by the European Research Council (ERC) Advanced Grant 101141363, ERC Proof of Concept Grant 101138728, Italian Association for Cancer Research (AIRC) Grants 19891 and 22737, Italian Ministry for University and Research Grants PE00000007 (INF-ACT) and PRIN 2022FMESXL, Funded Research Agreement from Asher Biotherapeutics, VIR Biotechnology, and BlueJay Therapeutics. V.F. is supported by the Italian Ministry for University and Research Grants PE00000007 (INF-ACT) and Fondazione Prossimo Mio.

AUTHOR CONTRIBUTIONS

K.S., A.V., and S.M. conceived and designed the experiments. B.K., I.S., K.S., C.D., M.S., and J.B. performed intravital epifluorescence microscopy. S.S., K.S., T.-D.T., and S.C. planned and performed histological and immunohistochemical analysis. J.B. and B.E. performed and analyzed TEM. S.S. and F.G. performed aggregometry. M.B.M., J.S., and B.K. performed flow chamber experiments. B.K., J.B., M.-L.v.B, J.S., F.S., and I.S. did surgery for IVC flow reduction in mice. B.K. and M.L. performed cell culture experiments. B.K. and S.S. performed flow cytometry experiments. A.L. and F.N. designed and performed immune complex binding experiments. V.F. and M.I. designed and performed SARS-CoV-2 infection experiments. L.P.F. and A.d.P.G. provided *Fcmr*$^{fl/fl}$ mice. M.M. provided antibodies. B.H. provided Cμ13 mice. C.Q.S. and A.D. provided Crry. M.R. provided lung autopsy specimens from COVID-19 patients. K.P., A.L., and L.N. provided plasma samples from COVID-19 patients. O.P., M.K., and P.M. performed proteome analysis. T.K. provided human vein specimens. K.S., A.V., and S.M. analyzed the data and composed the manuscript, and all authors reviewed it.

DECLARATION OF INTERESTS

C.Q.S. and A.D. are inventors of a patent application that describes the use of engineered proteins as potent complement regulators for therapeutic applications. C.Q.S. received honoraria for speaking at symposia organized by Alexion Pharmaceuticals and Swedish Orphan Biovitrum (Sobi). M.I. participates in advisory boards/consultantship for Asher Biotherapeutics, GentiBio, Clexio Biosciences, Sybilla Biotech, BlueJay Therapeutics, Bristol Myers Squibb, and Aligos Therapeutics and receives funding from Asher Biotherapeutics and VIR Biotechnology.

STAR★METHODS

Detailed methods are provided in the online version of this paper and include the following:

- KEY RESOURCES TABLE
- EXPERIMENTAL MODEL AND STUDY PARTICIPANT DETAILS
  - Animals
  - Generation of *Fcmr*$^{fl/fl}$ mice
  - Endothelial cell culture
  - Human thrombi and veins
- METHOD DETAILS
  - Mouse model of flow restriction in the IVC
  - Microvascular thrombosis model
  - Intravital epifluorescence microscopy
  - Immunofluorescence staining of frozen and paraffin embedded sections
  - Light transmission aggregometry
  - Flow cytometry of platelet-antibody interaction
  - Antibody deposition assay
  - Enzyme-linked Immunosorbent Assay
  - Thromboelastometry
  - Tail bleeding assay
  - Endothelial cell culture

- Flow cytometry of MVECs
- Flow cytometry for Fcμ Receptor expression on HUVECs and HSaVECs
- Chimera generation
- Proteome analysis
- Flow chamber experiments
- rtPCR
- rtPCR for IgM receptors in endothelial cells
- Western Blot
- Recombinant expression and purification of the murine complement inhibitor Crry
- NETosis assay
- SARS-CoV-2 infection mouse model combined with C1q and C3 complement component depletion
- Interaction of murine IgG immune complexes with FcμR-GFP Hek cells

- QUANTIFICATION AND STATISTICAL ANALYSIS

SUPPLEMENTAL INFORMATION

Supplemental information can be found online at https://doi.org/10.1016/j.immuni.2024.08.007.

Received: May 7, 2024
Revised: May 17, 2024
Accepted: August 7, 2024
Published: September 2, 2024

REFERENCES

1. Ehrenstein, M.R., and Notley, C.A. (2010). The importance of natural IgM: scavenger, protector and regulator. Nat. Rev. Immunol. *10*, 778–786. https://doi.org/10.1038/nri2849.
2. Elvin, J.G., Couston, R.G., and van der Walle, C.F. (2013). Therapeutic antibodies: market considerations, disease targets and bioprocessing. Int. J. Pharm. *440*, 83–98. https://doi.org/10.1016/j.ijpharm.2011.12.039.
3. Aggarwal, R., Charles-Schoeman, C., Schessl, J., Bata-Csörgő, Z., Dimachkie, M.M., Griger, Z., Moiseev, S., Oddis, C., Schiopu, E., Vencovský, J., et al. (2022). Trial of Intravenous Immune Globulin in Dermatomyositis. N. Engl. J. Med. *387*, 1264–1278. https://doi.org/10.1056/NEJMoa2117912.
4. Alahmari, A.K., Almalki, Z.S., Alahmari, A.K., and Guo, J.J. (2016). Thromboembolic Events Associated with Bevacizumab plus Chemotherapy for Patients with Colorectal Cancer: A Meta-Analysis of Randomized Controlled Trials. Am. Health Drug Benefits *9*, 221–232.
5. Ammann, E.M., Jones, M.P., Link, B.K., Carnahan, R.M., Winiecki, S.K., Torner, J.C., McDowell, B.D., Fireman, B.H., and Chrischilles, E.A. (2016). Intravenous immune globulin and thromboembolic adverse events in patients with hematologic malignancy. Blood *127*, 200–207. https://doi.org/10.1182/blood-2015-05-647552.
6. Cumpelik, A., Gerossier, E., Jin, J., Tsakiris, D., Dickenmann, M., Sadallah, S., Schifferli, J.A., and Zecher, D. (2015). Mechanism of Platelet Activation and Hypercoagulability by Antithymocyte Globulins (ATG). Am. J. Transplant. *15*, 2588–2601. https://doi.org/10.1111/ajt.13316.
7. Daniel, G.W., Menis, M., Sridhar, G., Scott, D., Wallace, A.E., Ovanesov, M.V., Golding, B., Anderson, S.A., Epstein, J., Martin, D., et al. (2012). Immune globulins and thrombotic adverse events as recorded in a large administrative database in 2008 through 2010. Transfusion *52*, 2113–2121. https://doi.org/10.1111/j.1537-2995.2012.03589.x.
8. Gupta, D., Shukla, P., Bisht, S.S., Bhatt, M.L., Pant, M.C., and Srivastava, K. (2011). Deep vein and artery thrombosis associated with cetuximab-based chemoradiotherapy. Indian J. Pharmacol. *43*, 478–480. https://doi.org/10.4103/0253-7613.83135.
9. Jin, P.H., Shin, S.C., and Dhamoon, M.S. (2020). Risk of thrombotic events after inpatient intravenous immunoglobulin or plasma exchange for neurologic disease: A case-crossover study. Muscle Nerve *62*, 327–332. https://doi.org/10.1002/mus.26884.
10. Marie, I., Maurey, G., Hervé, F., Hellot, M.F., and Levesque, H. (2006). Intravenous immunoglobulin-associated arterial and venous thrombosis; report of a series and review of the literature. Br. J. Dermatol. *155*, 714–721. https://doi.org/10.1111/j.1365-2133.2006.07390.x.
11. Mathis, A.S., and Rao, V. (2004). Deep vein thrombosis during rabbit antithymocyte globulin administration. Transplant. Proc. *36*, 3250–3251. https://doi.org/10.1016/j.transproceed.2004.09.086.
12. Menis, M., Sridhar, G., Selvam, N., Ovanesov, M.V., Divan, H.A., Liang, Y., Scott, D., Golding, B., Forshee, R., Ball, R., et al. (2013). Hyperimmune globulins and same-day thrombotic adverse events as recorded in a large healthcare database during 2008–2011. Am. J. Hematol. *88*, 1035–1040. https://doi.org/10.1002/ajh.23559.
13. Miroddi, M., Sterrantino, C., Simmonds, M., Caridi, L., Calapai, G., Phillips, R.S., and Stewart, L.A. (2016). Systematic review and meta-analysis of the risk of severe and life-threatening thromboembolism in cancer patients receiving anti-EGFR monoclonal antibodies (cetuximab or panitumumab). Int. J. Cancer *139*, 2370–2380. https://doi.org/10.1002/ijc.30280.
14. Petrelli, F., Cabiddu, M., Borgonovo, K., and Barni, S. (2012). Risk of venous and arterial thromboembolic events associated with anti-EGFR agents: a meta-analysis of randomized clinical trials. Ann. Oncol. *23*, 1672–1679. https://doi.org/10.1093/annonc/mdr592.
15. Weber, M., Kröger, N., Langer, F., Hansen, A., Zabelina, T., Eifrig, B., Hossfeld, D.K., and Zander, A.R. (2003). Non-overt disseminated intravascular coagulation in patients during treatment with antithymocyte globulin for unrelated allogeneic hematopoietic stem cell transplantation. Bone Marrow Transplant. *31*, 817–822. https://doi.org/10.1038/sj.bmt.1703921.
16. Greinacher, A. (2015). Heparin-Induced Thrombocytopenia. N. Engl. J. Med. *373*, 1883–1884. https://doi.org/10.1056/NEJMc1510993.
17. Greinacher, A., Thiele, T., Warkentin, T.E., Weisser, K., Kyrle, P.A., and Eichinger, S. (2021). Thrombotic Thrombocytopenia after ChAdOx1 nCov-19 Vaccination. N. Engl. J. Med. *384*, 2092–2101. https://doi.org/10.1056/NEJMoa2104840.
18. Kristinsson, S.Y., Pfeiffer, R.M., Björkholm, M., Goldin, L.R., Schulman, S., Blimark, C., Mellqvist, U.H., Wahlin, A., Turesson, I., and Landgren, O. (2010). Arterial and venous thrombosis in monoclonal gammopathy of undetermined significance and multiple myeloma: a population-based study. Blood *115*, 4991–4998. https://doi.org/10.1182/blood-2009-11-252072.
19. Leebeek, F.W.G. (2016). Update of thrombosis in multiple myeloma. Thromb. Res. *140*, S76–S80. https://doi.org/10.1016/S0049-3848(16)30103-7.
20. Meroni, P.L., Borghi, M.O., Raschi, E., and Tedesco, F. (2011). Pathogenesis of antiphospholipid syndrome: understanding the antibodies. Nat. Rev. Rheumatol. *7*, 330–339. https://doi.org/10.1038/nrrheum.2011.52.
21. Nørgaard, I., Nielsen, S.F., and Nordestgaard, B.G. (2016). Complement C3 and High Risk of Venous Thromboembolism: 80517 Individuals from the Copenhagen General Population Study. Clin. Chem. *62*, 525–534. https://doi.org/10.1373/clinchem.2015.251314.
22. Klok, F.A., Kruip, M.J.H.A., van der Meer, N.J.M., Arbous, M.S., Gommers, D., Kant, K.M., Kaptein, F.H.J., van Paassen, J., Stals, M.A.M., Huisman, M.V., et al. (2020). Confirmation of the high cumulative incidence of thrombotic complications in critically ill ICU patients with COVID-19: An updated analysis. Thromb. Res. *191*, 148–150. https://doi.org/10.1016/j.thromres.2020.04.041.
23. Ramlall, V., Thangaraj, P.M., Meydan, C., Foox, J., Butler, D., Kim, J., May, B., De Freitas, J.K., Glicksberg, B.S., Mason, C.E., et al. (2020). Immune complement and coagulation dysfunction in adverse outcomes of SARS-CoV-2 infection. Nat. Med. *26*, 1609–1615. https://doi.org/10.1038/s41591-020-1021-2.

24. Zhang, L., Feng, X., Zhang, D., Jiang, C., Mei, H., Wang, J., Zhang, C., Li, H., Xia, X., Kong, S., et al. (2020). Deep Vein Thrombosis in Hospitalized Patients With COVID-19 in Wuhan, China: Prevalence, Risk Factors, and Outcome. Circulation *142*, 114–128. https://doi.org/10.1161/CIRCULATIONAHA.120.046702.

25. Noris, M., Mescia, F., and Remuzzi, G. (2012). STEC-HUS, atypical HUS and TTP are all diseases of complement activation. Nat. Rev. Nephrol. *8*, 622–633. https://doi.org/10.1038/nrneph.2012.195.

26. Barcellini, W., Fattizzo, B., Zaninoni, A., Radice, T., Nichele, I., Di Bona, E., Lunghi, M., Tassinari, C., Alfinito, F., Ferrari, A., et al. (2014). Clinical heterogeneity and predictors of outcome in primary autoimmune hemolytic anemia: a GIMEMA study of 308 patients. Blood *124*, 2930–2936. https://doi.org/10.1182/blood-2014-06-583021.

27. Lood, C., Eriksson, S., Gullstrand, B., Jönsen, A., Sturfelt, G., Truedsson, L., and Bengtsson, A.A. (2012). Increased C1q, C4 and C3 deposition on platelets in patients with systemic lupus erythematosus–a possible link to venous thrombosis? Lupus *21*, 1423–1432. https://doi.org/10.1177/0961203312457210.

28. Hillmen, P., Young, N.S., Schubert, J., Brodsky, R.A., Socié, G., Muus, P., Röth, A., Szer, J., Elebute, M.O., Nakamura, R., et al. (2006). The complement inhibitor eculizumab in paroxysmal nocturnal hemoglobinuria. N. Engl. J. Med. *355*, 1233–1243. https://doi.org/10.1056/NEJMoa061648.

29. Kelly, R.J., Hill, A., Arnold, L.M., Brooksbank, G.L., Richards, S.J., Cullen, M., Mitchell, L.D., Cohen, D.R., Gregory, W.M., and Hillmen, P. (2011). Long-term treatment with eculizumab in paroxysmal nocturnal hemoglobinuria: sustained efficacy and improved survival. Blood *117*, 6786–6792. https://doi.org/10.1182/blood-2011-02-333997.

30. Legendre, C.M., Licht, C., Muus, P., Greenbaum, L.A., Babu, S., Bedrosian, C., Bingham, C., Cohen, D.J., Delmas, Y., Douglas, K., et al. (2013). Terminal complement inhibitor eculizumab in atypical hemolytic-uremic syndrome. N. Engl. J. Med. *368*, 2169–2181. https://doi.org/10.1056/NEJMoa1208981.

31. Józsi, M., Licht, C., Strobel, S., Zipfel, S.L.H., Richter, H., Heinen, S., Zipfel, P.F., and Skerka, C. (2008). Factor H autoantibodies in atypical hemolytic uremic syndrome correlate with CFHR1/CFHR3 deficiency. Blood *111*, 1512–1514. https://doi.org/10.1182/blood-2007-09-109876.

32. Stark, K., Philippi, V., Stockhausen, S., Busse, J., Antonelli, A., Miller, M., Schubert, I., Hoseinpour, P., Chandraratne, S., von Brühl, M.L., et al. (2016). Disulfide HMGB1 derived from platelets coordinates venous thrombosis in mice. Blood *128*, 2435–2449. https://doi.org/10.1182/blood-2016-04-710632.

33. Iovino, F., Engelen-Lee, J.Y., Brouwer, M., van de Beek, D., van der Ende, A., Valls Seron, M., Mellroth, P., Muschiol, S., Bergstrand, J., Widengren, J., et al. (2017). pIgR and PECAM-1 bind to pneumococcal adhesins RrgA and PspC mediating bacterial brain invasion. J. Exp. Med. *214*, 1619–1630. https://doi.org/10.1084/jem.20161668.

34. Diebolder, C.A., Beurskens, F.J., de Jong, R.N., Koning, R.I., Strumane, K., Lindorfer, M.A., Voorhorst, M., Ugurlar, D., Rosati, S., Heck, A.J.R., et al. (2014). Complement is activated by IgG hexamers assembled at the cell surface. Science *343*, 1260–1263. https://doi.org/10.1126/science.1248943.

35. Wang, G., de Jong, R.N., van den Bremer, E.T.J., Beurskens, F.J., Labrijn, A.F., Ugurlar, D., Gros, P., Schuurman, J., Parren, P.W.H.I., and Heck, A.J.R. (2016). Molecular Basis of Assembly and Activation of Complement Component C1 in Complex with Immunoglobulin G1 and Antigen. Mol. Cell *63*, 135–145. https://doi.org/10.1016/j.molcel.2016.05.016.

36. Nguyen, T.T.T., Kläsener, K., Zürn, C., Castillo, P.A., Brust-Mascher, I., Imai, D.M., Bevins, C.L., Reardon, C., Reth, M., and Baumgarth, N. (2017). The IgM receptor FcμR limits tonic BCR signaling by regulating expression of the IgM BCR. Nat. Immunol. *18*, 321–333. https://doi.org/10.1038/ni.3677.

37. Kilani, B., Gourdou-Latyszenok, V., Guy, A., Bats, M.L., Peghaire, C., Parrens, M., Renault, M.A., Duplàa, C., Villeval, J.L., Rautou, P.E., et al. (2019). Comparison of endothelial promoter efficiency and specificity in mice reveals a subset of Pdgfb-positive hematopoietic cells. J. Thromb. Haemost. *17*, 827–840. https://doi.org/10.1111/jth.14417.

38. Poisson, J., Tanguy, M., Davy, H., Camara, F., El Mdawar, M.B., Kheloufi, M., Dagher, T., Devue, C., Lasselin, J., Plessier, A., et al. (2020). Erythrocyte-derived microvesicles induce arterial spasms in JAK2V617F myeloproliferative neoplasm. J. Clin. Invest. *130*, 2630–2643. https://doi.org/10.1172/JCI124566.

39. Hangartner, L., Senn, B.M., Ledermann, B., Kalinke, U., Seiler, P., Bucher, E., Zellweger, R.M., Fink, K., Odermatt, B., Bürki, K., et al. (2003). Antiviral immune responses in gene-targeted mice expressing the immunoglobulin heavy chain of virus-neutralizing antibodies. Proc. Natl. Acad. Sci. USA *100*, 12883–12888. https://doi.org/10.1073/pnas.2135542100.

40. Coulie, P.G., and Van Snick, J. (1985). Enhancement of IgG anti-carrier responses by IgG2 anti-hapten antibodies in mice. Eur. J. Immunol. *15*, 793–798. https://doi.org/10.1002/eji.1830150810.

41. Heyman, B., Wiersma, E., and Nose, M. (1988). Complement activation is not required for IgG-mediated suppression of the antibody response. Eur. J. Immunol. *18*, 1739–1743. https://doi.org/10.1002/eji.1830181113.

42. Wiersma, E.J., Coulie, P.G., and Heyman, B. (1989). Dual immunoregulatory effects of monoclonal IgG-antibodies: suppression and enhancement of the antibody response. Scand. J. Immunol. *29*, 439–448. https://doi.org/10.1111/j.1365-3083.1989.tb01143.x.

43. Wiersma, E.J., Nose, M., and Heyman, B. (1990). Evidence of IgG-mediated enhancement of the antibody response in vivo without complement activation via the classical pathway. Eur. J. Immunol. *20*, 2585–2589. https://doi.org/10.1002/eji.1830201209.

44. Brill, A., Fuchs, T.A., Savchenko, A.S., Thomas, G.M., Martinod, K., De Meyer, S.F., Bhandari, A.A., and Wagner, D.D. (2012). Neutrophil extracellular traps promote deep vein thrombosis in mice. J. Thromb. Haemost. *10*, 136–144. https://doi.org/10.1111/j.1538-7836.2011.04544.x.

45. Martinod, K., Demers, M., Fuchs, T.A., Wong, S.L., Brill, A., Gallant, M., Hu, J., Wang, Y., and Wagner, D.D. (2013). Neutrophil histone modification by peptidylarginine deiminase 4 is critical for deep vein thrombosis in mice. Proc. Natl. Acad. Sci. USA *110*, 8674–8679. https://doi.org/10.1073/pnas.1301059110.

46. von Brühl, M.L., Stark, K., Steinhart, A., Chandraratne, S., Konrad, I., Lorenz, M., Khandoga, A., Tirniceriu, A., Coletti, R., Köllnberger, M., et al. (2012). Monocytes, neutrophils, and platelets cooperate to initiate and propagate venous thrombosis in mice in vivo. J. Exp. Med. *209*, 819–835. https://doi.org/10.1084/jem.20112322.

47. Nader, H.B. (1991). Characterization of a heparan sulfate and a peculiar chondroitin 4-sulfate proteoglycan from platelets. Inhibition of the aggregation process by platelet chondroitin sulfate proteoglycan. J. Biol. Chem. *266*, 10518–10523.

48. Hamad, O.A., Nilsson, P.H., Lasaosa, M., Ricklin, D., Lambris, J.D., Nilsson, B., and Ekdahl, K.N. (2010). Contribution of chondroitin sulfate A to the binding of complement proteins to activated platelets. PLoS One *5*, e12889. https://doi.org/10.1371/journal.pone.0012889.

49. Imada, T., Saito, Y., and Inada, Y. (1981). Domains in serum albumin responsible for platelet aggregation. FEBS Lett. *134*, 249–252. https://doi.org/10.1016/0014-5793(81)80612-6.

50. Verschoor, A., Neuenhahn, M., Navarini, A.A., Graef, P., Plaumann, A., Seidlmeier, A., Nieswandt, B., Massberg, S., Zinkernagel, R.M., Hengartner, H., et al. (2011). A platelet-mediated system for shuttling blood-borne bacteria to CD8α+ dendritic cells depends on glycoprotein GPIb and complement C3. Nat. Immunol. *12*, 1194–1201. https://doi.org/10.1038/ni.2140.

51. Hamad, O.A., Mitroulis, I., Fromell, K., Kozarcanin, H., Chavakis, T., Ricklin, D., Lambris, J.D., Ekdahl, K.N., and Nilsson, B. (2015). Contact activation of C3 enables tethering between activated platelets and polymorphonuclear leukocytes via CD11b/CD18. Thromb. Haemost. *114*, 1207–1217. https://doi.org/10.1160/TH15-02-0162.

52. Chang, S.L., Huang, Y.L., Lee, M.C., Hu, S., Hsiao, Y.C., Chang, S.W., Chang, C.J., and Chen, P.C. (2018). Association of Varicose Veins With Incident Venous Thromboembolism and Peripheral Artery Disease. JAMA *319*, 807–817. https://doi.org/10.1001/jama.2018.0246.

53. Langer, F., Spath, B., Fischer, C., Stolz, M., Ayuk, F.A., Kröger, N., Bokemeyer, C., and Ruf, W. (2013). Rapid activation of monocyte tissue factor by antithymocyte globulin is dependent on complement and protein disulfide isomerase. Blood *121*, 2324–2335. https://doi.org/10.1182/blood-2012-10-460493.

54. Nalluri, S.R., Chu, D., Keresztes, R., Zhu, X., and Wu, S. (2008). Risk of venous thromboembolism with the angiogenesis inhibitor bevacizumab in cancer patients: a meta-analysis. JAMA *300*, 2277–2285. https://doi.org/10.1001/jama.2008.656.

55. Kurtovic, L., and Beeson, J.G. (2021). Complement Factors in COVID-19 Therapeutics and Vaccines. Trends Immunol. *42*, 94–103. https://doi.org/10.1016/j.it.2020.12.002.

56. Brill, A., Fuchs, T.A., Chauhan, A.K., Yang, J.J., De Meyer, S.F., Köllnberger, M., Wakefield, T.W., Lämmle, B., Massberg, S., and Wagner, D.D. (2011). von Willebrand factor-mediated platelet adhesion is critical for deep vein thrombosis in mouse models. Blood *117*, 1400–1407. https://doi.org/10.1182/blood-2010-05-287623.

57. Tomar, D.S., Kumar, S., Singh, S.K., Goswami, S., and Li, L. (2016). Molecular basis of high viscosity in concentrated antibody solutions: Strategies for high concentration drug product development. mAbs *8*, 216–228. https://doi.org/10.1080/19420862.2015.1128606.

58. Nieba, L., Nieba-Axmann, S.E., Persson, A., Hämäläinen, M., Edebratt, F., Hansson, A., Lidholm, J., Magnusson, K., Karlsson, A.F., and Plückthun, A. (1997). BIACORE analysis of histidine-tagged proteins using a chelating NTA sensor chip. Anal. Biochem. *252*, 217–228. https://doi.org/10.1006/abio.1997.2326.

59. Nyamboya, R.A., Sutton, B.J., and Calvert, R.A. (2020). Mapping of the binding site for FcμR in human IgM-Fc. Biochim. Biophys. Acta Proteins Proteom. *1868*, 140266. https://doi.org/10.1016/j.bbapap.2019.140266.

60. Haas, M.S., Alicot, E.M., Schuerpf, F., Chiu, I., Li, J., Moore, F.D., and Carroll, M.C. (2010). Blockade of self-reactive IgM significantly reduces injury in a murine model of acute myocardial infarction. Cardiovasc. Res. *87*, 618–627. https://doi.org/10.1093/cvr/cvq141.

61. Holers, V.M., and Kulik, L. (2007). Complement receptor 2, natural antibodies and innate immunity: Inter-relationships in B cell selection and activation. Mol. Immunol. *44*, 64–72. https://doi.org/10.1016/j.molimm.2006.07.003.

62. Ouchida, R., Mori, H., Hase, K., Takatsu, H., Kurosaki, T., Tokuhisa, T., Ohno, H., and Wang, J.Y. (2012). Critical role of the IgM Fc receptor in IgM homeostasis, B-cell survival, and humoral immune responses. Proc. Natl. Acad. Sci. USA *109*, E2699–E2706. https://doi.org/10.1073/pnas.1210706109.

63. Manukyan, D., Müller-Calleja, N., Jäckel, S., Luchmann, K., Mönnikes, R., Kiouptsi, K., Reinhardt, C., Jurk, K., Walter, U., and Lackner, K.J. (2016). Cofactor-independent human antiphospholipid antibodies induce venous thrombosis in mice. J. Thromb. Haemost. *14*, 1011–1020. https://doi.org/10.1111/jth.13263.

64. Müller-Calleja, N., Hollerbach, A., Royce, J., Ritter, S., Pedrosa, D., Madhusudhan, T., Teifel, S., Meineck, M., Häuser, F., Canisius, A., et al. (2021). Lipid presentation by the protein C receptor links coagulation with autoimmunity. Science *371*, eabc0956. https://doi.org/10.1126/science.abc0956.

65. Zhou, Y., Abraham, S., Andre, P., Edelstein, L.C., Shaw, C.A., Dangelmaier, C.A., Tsygankov, A.Y., Kunapuli, S.P., Bray, P.F., and McKenzie, S.E. (2015). Anti-miR-148a regulates platelet FcγRIIA signaling and decreases thrombosis in vivo in mice. Blood *126*, 2871–2881. https://doi.org/10.1182/blood-2015-02-631135.

66. Andersson, J., Ekdahl, K.N., Lambris, J.D., and Nilsson, B. (2005). Binding of C3 fragments on top of adsorbed plasma proteins during complement activation on a model biomaterial surface. Biomaterials *26*, 1477–1485. https://doi.org/10.1016/j.biomaterials.2004.05.011.

67. Gorbet, M.B., and Sefton, M.V. (2004). Biomaterial-associated thrombosis: roles of coagulation factors, complement, platelets and leukocytes. Biomaterials *25*, 5681–5703. https://doi.org/10.1016/j.biomaterials.2004.01.023.

68. Nilsson, B., Ekdahl, K.N., Mollnes, T.E., and Lambris, J.D. (2007). The role of complement in biomaterial-induced inflammation. Mol. Immunol. *44*, 82–94. https://doi.org/10.1016/j.molimm.2006.06.020.

69. Wetterö, J., Bengtsson, T., and Tengvall, P. (2000). Complement activation on immunoglobulin G-coated hydrophobic surfaces enhances the release of oxygen radicals from neutrophils through an actin-dependent mechanism. J. Biomed. Mater. Res. *51*, 742–751. https://doi.org/10.1002/1097-4636(20000915)51:4<742::aid-jbm24>3.0.co;2-d.

70. Boehm, T.K., Sojar, H., and Denardin, E. (2010). Concentration-dependent effect of fibrinogen on IgG-specific antigen binding and phagocytosis. Cell. Immunol. *263*, 41–48. https://doi.org/10.1016/j.cellimm.2010.02.014.

71. Broadley, S.P., Plaumann, A., Coletti, R., Lehmann, C., Wanisch, A., Seidlmeier, A., Esser, K., Luo, S., Rämer, P.C., Massberg, S., et al. (2016). Dual-Track Clearance of Circulating Bacteria Balances Rapid Restoration of Blood Sterility with Induction of Adaptive Immunity. Cell Host Microbe *20*, 36–48. https://doi.org/10.1016/j.chom.2016.05.023.

72. Engelmann, B., and Massberg, S. (2013). Thrombosis as an intravascular effector of innate immunity. Nat. Rev. Immunol. *13*, 34–45. https://doi.org/10.1038/nri3345.

73. Gaertner, F., Ahmad, Z., Rosenberger, G., Fan, S., Nicolai, L., Busch, B., Yavuz, G., Luckner, M., Ishikawa-Ankerhold, H., Hennel, R., et al. (2017). Migrating Platelets Are Mechano-scavengers that Collect and Bundle Bacteria. Cell *171*, 1368–1382.e23. https://doi.org/10.1016/j.cell.2017.11.001.

74. Schmidt, C.Q., and Verschoor, A. (2017). Complement and coagulation: so close, yet so far. Blood *130*, 2581–2582. https://doi.org/10.1182/blood-2017-10-811943.

75. Verschoor, A., and Langer, H.F. (2013). Crosstalk between platelets and the complement system in immune protection and disease. Thromb. Haemost. *110*, 910–919. https://doi.org/10.1160/TH13-02-0102.

76. Ackermann, M., Verleden, S.E., Kuehnel, M., Haverich, A., Welte, T., Laenger, F., Vanstapel, A., Werlein, C., Stark, H., Tzankov, A., et al. (2020). Pulmonary Vascular Endothelialitis, Thrombosis, and Angiogenesis in Covid-19. N. Engl. J. Med. *383*, 120–128. https://doi.org/10.1056/NEJMoa2015432.

77. Malas, M.B., Naazie, I.N., Elsayed, N., Mathlouthi, A., Marmor, R., and Clary, B. (2020). Thromboembolism risk of COVID-19 is high and associated with a higher risk of mortality: A systematic review and meta-analysis. EClinicalMedicine *29*, 100639. https://doi.org/10.1016/j.eclinm.2020.100639.

78. Nicolai, L., Leunig, A., Brambs, S., Kaiser, R., Weinberger, T., Weigand, M., Muenchhoff, M., Hellmuth, J.C., Ledderose, S., Schulz, H., et al. (2020). Immunothrombotic Dysregulation in COVID-19 Pneumonia Is Associated With Respiratory Failure and Coagulopathy. Circulation *142*, 1176–1189. https://doi.org/10.1161/CIRCULATIONAHA.120.048488.

79. Peerschke, E.I., and Ghebrehiwet, B. (1997). C1q augments platelet activation in response to aggregated Ig. J. Immunol. *159*, 5594–5598.

80. Mannes, M., Pechtl, V., Hafner, S., Dopler, A., Eriksson, O., Manivel, V.A., Wohlgemuth, L., Messerer, D.A.C., Schrezenmeier, H., Ekdahl, K.N., et al. (2023). Complement and platelets: prothrombotic cell activation requires membrane attack complex-induced release of danger signals. Blood Adv. *7*, 6367–6380. https://doi.org/10.1182/bloodadvances.2023010817.

81. Mastellos, D.C., Ricklin, D., and Lambris, J.D. (2019). Clinical promise of next-generation complement therapeutics. Nat. Rev. Drug Discov. *18*, 707–729. https://doi.org/10.1038/s41573-019-0031-6.

82. Gushiken, F.C., Han, H., Li, J., Rumbaut, R.E., and Afshar-Kharghan, V. (2009). Abnormal platelet function in C3-deficient mice. J. Thromb. Haemost. *7*, 865–870. https://doi.org/10.1111/j.1538-7836.2009.03334.x.

83. Guo, Y., Tian, X., Wang, X., and Xiao, Z. (2018). Adverse Effects of Immunoglobulin Therapy. Front. Immunol. *9*, 1299. https://doi.org/10.3389/fimmu.2018.01299.

84. Huang, L., Kanellis, J., and Mulley, W. (2011). Slow and steady. Reducing thrombotic events in renal transplant recipients treated with IVIg for antibody-mediated rejection. Nephrology (Carlton) *16*, 239–242. https://doi.org/10.1111/j.1440-1797.2010.01399.x.

85. Fumagalli, V., Ravà, M., Marotta, D., Di Lucia, P., Bono, E.B., Giustini, L., De Leo, F., Casalgrandi, M., Monteleone, E., Mouro, V., et al. (2024). Antibody-independent protection against heterologous SARS-CoV-2 challenge conferred by prior infection or vaccination. Nat. Immunol. *25*, 633–643. https://doi.org/10.1038/s41590-024-01787-z.

86. Fumagalli, V., Ravà, M., Marotta, D., Di Lucia, P., Laura, C., Sala, E., Grillo, M., Bono, E., Giustini, L., Perucchini, C., et al. (2022). Administration of aerosolized SARS-CoV-2 to K18-hACE2 mice uncouples respiratory infection from fatal neuroinvasion. Sci. Immunol. *7*, eabl9929. https://doi.org/10.1126/sciimmunol.abl9929.

87. Schmidt, C.Q., Slingsby, F.C., Richards, A., and Barlow, P.N. (2011). Production of biologically active complement factor H in therapeutically useful quantities. Protein Expr. Purif. *76*, 254–263. https://doi.org/10.1016/j.pep.2010.12.002.

88. Mombaerts, P., Iacomini, J., Johnson, R.S., Herrup, K., Tonegawa, S., and Papaioannou, V.E. (1992). RAG-1-deficient mice have no mature B and T lymphocytes. Cell *68*, 869–877. https://doi.org/10.1016/0092-8674(92)90030-g.

89. Roopenian, D.C., Low, B.E., Christianson, G.J., Proetzel, G., Sproule, T.J., and Wiles, M.V. (2015). Albumin-deficient mouse models for studying metabolism of human albumin and pharmacokinetics of albumin-based drugs. mAbs *7*, 344–351. https://doi.org/10.1080/19420862.2015.1008345.

90. Shi, L., Takahashi, K., Dundee, J., Shahroor-Karni, S., Thiel, S., Jensenius, J.C., Gad, F., Hamblin, M.R., Sastry, K.N., and Ezekowitz, R.A.B. (2004). Mannose-binding lectin-deficient mice are susceptible to infection with Staphylococcus aureus. J. Exp. Med. *199*, 1379–1390. https://doi.org/10.1084/jem.20032207.

91. Boes, M., Esau, C., Fischer, M.B., Schmidt, T., Carroll, M., and Chen, J. (1998). Enhanced B-1 cell development, but impaired IgG antibody responses in mice deficient in secreted IgM. J. Immunol. *160*, 4776–4787.

92. Kumazaki, K., Tirosh, B., Maehr, R., Boes, M., Honjo, T., and Ploegh, H.L. (2007). AID-/-mus-/- mice are agammaglobulinemic and fail to maintain B220-CD138+ plasma cells. J. Immunol. *178*, 2192–2203.

93. Botto, M., Dell'Agnola, C., Bygrave, A.E., Thompson, E.M., Cook, H.T., Petry, F., Loos, M., Pandolfi, P.P., and Walport, M.J. (1998). Homozygous C1q deficiency causes glomerulonephritis associated with multiple apoptotic bodies. Nat. Genet. *19*, 56–59. https://doi.org/10.1038/ng0598-56.

94. Pekna, M., Hietala, M.A., Landin, A., Nilsson, A.K., Lagerberg, C., Betsholtz, C., and Pekny, M. (1998). Mice deficient for the complement factor B develop and reproduce normally. Scand. J. Immunol. *47*, 375–380.

95. Wessels, M.R., Butko, P., Ma, M., Warren, H.B., Lage, A.L., and Carroll, M.C. (1995). Studies of group B streptococcal infection in mice deficient in complement component C3 or C4 demonstrate an essential role for complement in both innate and acquired immunity. Proc. Natl. Acad. Sci. USA *92*, 11490–11494.

96. Fischer, M.B., Ma, M., Goerg, S., Zhou, X., Xia, J., Finco, O., Han, S., Kelsoe, G., Howard, R.G., Rothstein, T.L., et al. (1996). Regulation of the B cell response to T-dependent antigens by classical pathway complement. J. Immunol. *157*, 549–556.

97. Humbles, A.A., Lu, B., Nilsson, C.A., Lilly, C., Israel, E., Fujiwara, Y., Gerard, N.P., and Gerard, C. (2000). A role for the C3a anaphylatoxin receptor in the effector phase of asthma. Nature *406*, 998–1001. https://doi.org/10.1038/35023175.

98. Wetsel, R.A., Fleischer, D.T., and Haviland, D.L. (1990). Deficiency of the murine fifth complement component (C5). A 2-base pair gene deletion in a 5′-exon. J. Biol. Chem. *265*, 2435–2440.

99. Höpken, U.E., Lu, B., Gerard, N.P., and Gerard, C. (1996). The C5a chemoattractant receptor mediates mucosal defence to infection. Nature *383*, 86–89. https://doi.org/10.1038/383086a0.

100. Park, S.Y., Ueda, S., Ohno, H., Hamano, Y., Tanaka, M., Shiratori, T., Yamazaki, T., Arase, H., Arase, N., Karasawa, A., et al. (1998). Resistance of Fc receptor- deficient mice to fatal glomerulonephritis. J. Clin. Invest. *102*, 1229–1238. https://doi.org/10.1172/JCI3256.

101. van Montfoort, N., 't Hoen, P.A.C., Mangsbo, S.M., Camps, M.G.M., Boross, P., Melief, C.J.M., Ossendorp, F., and Verbeek, J.S. (2012). Fcgamma receptor IIb strongly regulates Fcgamma receptor-facilitated T cell activation by dendritic cells. J. Immunol. *189*, 92–101. https://doi.org/10.4049/jimmunol.1103703.

102. Lang, K.S., Lang, P.A., Meryk, A., Pandyra, A.A., Boucher, L.M., Pozdeev, V.I., Tusche, M.W., Göthert, J.R., Haight, J., Wakeham, A., et al. (2013). Involvement of Toso in activation of monocytes, macrophages, and granulocytes. Proc. Natl. Acad. Sci. USA *110*, 2593–2598. https://doi.org/10.1073/pnas.1222264110.

103. Molina, H., Holers, V.M., Li, B., Fung, Y., Mariathasan, S., Goellner, J., Strauss-Schoenberger, J., Karr, R.W., and Chaplin, D.D. (1996). Markedly impaired humoral immune response in mice deficient in complement receptors 1 and 2. Proc. Natl. Acad. Sci. USA *93*, 3357–3361.

104. Wu, H., Rodgers, J.R., Perrard, X.Y.D., Perrard, J.L., Prince, J.E., Abe, Y., Davis, B.K., Dietsch, G., Smith, C.W., and Ballantyne, C.M. (2004). Deficiency of CD11b or CD11d results in reduced staphylococcal enterotoxin-induced T cell response and T cell phenotypic changes. J. Immunol. *173*, 297–306.

105. Coxon, A., Rieu, P., Barkalow, F.J., Askari, S., Sharpe, A.H., von Andrian, U.H., Arnaout, M.A., and Mayadas, T.N. (1996). A novel role for the beta 2 integrin CD11b/CD18 in neutrophil apoptosis: a homeostatic mechanism in inflammation. Immunity *5*, 653–666.

106. Rutemark, C., Alicot, E., Bergman, A., Ma, M., Getahun, A., Ellmerich, S., Carroll, M.C., and Heyman, B. (2011). Requirement for complement in antibody responses is not explained by the classic pathway activator IgM. Proc. Natl. Acad. Sci. USA *108*, E934–E942. https://doi.org/10.1073/pnas.1109831108.

107. Tiedt, R., Schomber, T., Hao-Shen, H., and Skoda, R.C. (2007). Pf4-Cre transgenic mice allow the generation of lineage-restricted gene knockouts for studying megakaryocyte and platelet function in vivo. Blood *109*, 1503–1506. https://doi.org/10.1182/blood-2006-04-020362.

108. McKenzie, S.E., Taylor, S.M., Malladi, P., Yuhan, H., Cassel, D.L., Chien, P., Schwartz, E., Schreiber, A.D., Surrey, S., and Reilly, M.P. (1999). The role of the human Fc receptor Fc gamma RIIA in the immune clearance of platelets: a transgenic mouse model. J. Immunol. *162*, 4311–4318.

109. Chen, M.J., Yokomizo, T., Zeigler, B.M., Dzierzak, E., and Speck, N.A. (2009). Runx1 is required for the endothelial to haematopoietic cell transition but not thereafter. Nature *457*, 887–891. https://doi.org/10.1038/nature07619.

110. da Palma Guerreiro, A., Dorweiler, C., Halmer, I., Merkel, O., Hartmann, E.M., Berg, V., Reinart, N., Fingerle-Rowson, G., Knittel, G., Pallasch, C., et al. (2018). FcmR Shapes BCR Signaling in IgM-Positive Leukemia. Blood *132*, 2620. https://doi.org/10.1182/blood-2018-99-118352.

111. McCray, P.B., Jr., Pewe, L., Wohlford-Lenane, C., Hickey, M., Manzel, L., Shi, L., Netland, J., Jia, H.P., Halabi, C., Sigmund, C.D., et al. (2007). Lethal infection of K18-hACE2 mice infected with severe acute respiratory syndrome coronavirus. J. Virol. *81*, 813–821. https://doi.org/10.1128/JVI.02012-06.

112. Bromberger, T., Klapproth, S., Rohwedder, I., Zhu, L., Mittmann, L., Reichel, C.A., Sperandio, M., Qin, J., and Moser, M. (2018). Direct Rap1/Talin1 interaction regulates platelet and neutrophil integrin activity

in mice. Blood *132*, 2754–2762. https://doi.org/10.1182/blood-2018-04-846766.

113. Massberg, S., Brand, K., Grüner, S., Page, S., Müller, E., Müller, I., Bergmeier, W., Richter, T., Lorenz, M., Konrad, I., et al. (2002). A critical role of platelet adhesion in the initiation of atherosclerotic lesion formation. J. Exp. Med. *196*, 887–896.

114. Pekayvaz, K., Leunig, A., Kaiser, R., Joppich, M., Brambs, S., Janjic, A., Popp, O., Nixdorf, D., Fumagalli, V., Schmidt, N., et al. (2022). Protective immune trajectories in early viral containment of non-pneumonic SARS-CoV-2 infection. Nat. Commun. *13*, 1018. https://doi.org/10.1038/s41467-022-28508-0.

115. Yamamoto, K., Protack, C.D., Kuwahara, G., Tsuneki, M., Hashimoto, T., Hall, M.R., Assi, R., Brownson, K.E., Foster, T.R., Bai, H., et al. (2015). Disturbed shear stress reduces Klf2 expression in arterial-venous fistulae in vivo. Physiol. Rep. *3*, 3. https://doi.org/10.14814/phy2.12348.

116. Kurita, N., Honda, S.I., Usui, K., Shimizu, Y., Miyamoto, A., Tahara-Hanaoka, S., Shibuya, K., and Shibuya, A. (2009). Identification of the Fcalpha/muR isoform specifically expressed in the kidney tubules. Mol. Immunol. *46*, 749–753. https://doi.org/10.1016/j.molimm.2008.10.002.

STAR★METHODS

KEY RESOURCES TABLE

REAGENT or RESOURCE	SOURCE	IDENTIFIER
Antibodies		
Rat anti mouse C1q depleting antibody (clone RmC7H8)	BDBiosciences	Cat#757667; RRID: AB_10547924
Rat IgG1 Isotype control	Bioxcell	Cat#BE0290; RRID: AB_2687813
Mouse pooled polyclonal IgM	Rockland	Cat#010-0107; RRID: AB_840902
Mouse Pooled Polyclonal IgG	Jackson ImmunoResearch	Cat#015-000-002; RRID: AB_2337187
Mouse monoclonal anti-influenza A virus NP IgG2a (clone H16-L10-4R5 (HB65))	BioXcell	Cat#BE0159; RRID: AB_10949071
Mouse monoclonal anti-HIV gp120 IgG1 (clone 55-36)	BioXcell	Cat#BE0154; RRID: AB_10950313
Mouse monoclonal anti-KLH IgM	BioXcell	N/A
Mouse Fc-Fragment	BioXcell	Cat#BE0097; RRID: AB_1107787
Rat anti-mouse GPIbα (CD42b)	Emfret analytics	Cat#R300
Rat isotype IgG	Emfret analytics	N/A
Mouse anti-Fluorescein IgG1 Fc Silent™ (clone 4-4-20 (enhanced))	Absolute antibody	Cat#Ab00102-1.4
Mouse anti-Fluorescein IgG1 (clone 4-4-20 (enhanced))	Absolute antibody	Cat#Ab00102-1.1
Rat anti-Polymeric immunoglobulin receptor/PIGR inhibitor antibody (clone 7C1)	Abcam	Cat#ab170321
Mouse IgG1 anti-TNP non-complement activating antibody H5 mab (clone B8401H5)	Birgitta Heyman; Heyman et al.[41]	N/A
Mouse IgG1 Isotype control	Bioxcell	Cat#BE0083; RRID: AB_1107784
Rat anti mouse CD41 (clone MWReg30)	BD Biosciences	Cat#558040; RRID: AB_397004
Rabbit anti human Fibrin(-ogen)	DAKO	Cat#A0080; RRID: AB_2894406
Rat anti mouse Ly6G (clone 1A8)	ThermoFisher	Cat#12-9668-82; RRID: AB_2572720
Rabbit anti human MPO	DAKO	Cat#A0398; RRID: AB_2335676
Rat anti mouse F4/80 (clone Cl:A3-1)	Serotec (Bio-Rad)	Cat#MCA497; RRID: AB_2335599
Rat anti mouse complement C4 (clone 16D2)	ThermoFisher	Cat#MA1-40047; RRID: AB_1073827
Rabbit anti mouse CD42b	Abcam	Cat# ab104704; RRID: AB_10712312
Goat anti-Mouse IgM (Heavy chain) Cross-Adsorbed Secondary Antibody, Alexa Fluor™ 488	ThermoFisher	Cat#A21042; RRID: AB_2535711
Rabbit anti human FcμR	Sigma-Aldrich	Cat#HPA003910; RRID: AB_1078798
Rabbit anti human anti mouse vWF	Dako	Cat#A0082; RRID: AB_2315602
Rat anti mouse CD62P (clone RB40.34 (RUO))	BD Biosciences	Cat#553742; RRID: AB_2254315
Rabbit anti mouse ICAM1 (clone 020)	Sino biological	Cat#50440-R020; RRID: AB_2860508
Rat anti mouse CD31 (clone 390)	ThermoFisher	Cat#16-0311-85; RRID: AB_468933
Goat Alexa labeled F(ab)2-fragments anti mouse IgG Fcγ	Jackson Immunoresearch	Cat#115-546-071; RRID: AB_2338865
Goat F(ab')2 Anti-Human IgG - Fc (DyLight® 650), pre-adsorbed	Abcam	Cat#ab98593; RRID: AB_10674807
Goat DyLight-conjugated anti rat IgG	ThermoFisher	Cat#SA5-10021; RRID: AB_2556601
Mouse anti human CD42b (clone 42C01)	ThermoFisher	Cat#MA5-11642; RRID: AB_10986763
Rabbit anti human C4	Bioss	Cat#bs-15186R-A647; RRID: AB_374824
Rabbit anti human C1q-AF647	Bioss	Cat#bs-10750R-A647
Rabbit anti human C1q-AF488	Bioss	Cat#bs-10750R-A488
Goat anti human C3	Bioss	Cat#bs0367G-A647; RRID: AB_1604680
Mouse anti human CD31 (clone JC/70A)	ThermoFisher	Cat#MA5-13188; RRID: AB_10982120
Mouse FITC labeled IgM isotype control (clone: G155-228 (RUO))	BD Biosciences	Cat#553474; RRID: AB_10053771
Mouse FITC labeled IgG1 isotype control (clone: MOPC-31C (RUO))	BD Biosciences	Cat#550616; RRID: AB_479687
Rat anti mouse CD62P Ab (Clone RB40.34)	BD Biosciences	Cat#563674; RRID: AB_2738366

(*Continued on next page*)

Continued

REAGENT or RESOURCE	SOURCE	IDENTIFIER
Mouse anti human CD62P Ab (clone CLB-Thromb/6)	Immunotech (Beckman Coulter)	Cat#1759
Human isotype control IgG	antikoerper-online.de	Cat#ABIN964314
Rabbit anti mouse P-selectin	Biorbyt	Cat#orb385621
Goat anti-Rabbit IgG (H+L) Secondary Antibody, Alexa Fluor™ 594	Invitrogen	Cat#A-11012; RRID: AB_2534079
Goat anti mouse pIgR	R&D Systems	Cat#AF2800; RRID: AB_2283871
Hamster anti mouse ICAM-1	BD Biosciences	Cat#561898; RRID: AB_11153304
Mouse anti-Human Fcμ Receptor (clone HM14-1)	BD Biosciences	Cat#563017; RRID: AB_2737953
Mouse IgG1, κ Isotype Control (clone MOPC-31C)	BD Biosciences	Cat#550617; RRID: AB_10050483
Rabbit anti mouse FAIM3 Polyclonal Antibody	Bioss	Cat#bs-7527R
Goat anti-Rabbit IgG (H+L) Secondary Antibody, HRP	ThermoFisher	Cat#31460; RRID: AB_228341
TNP-specific murine IgG1 (clone 7B4)	Birgitta Heyman; Wiersma et al.[42]	N/A
Goat anti-mouse IgG-Fc F(ab)2	Jackson Immunoresearch	Cat#115-116; RRID: AB_2338629
Bacterial and virus strains		
SARS-CoV-2/human/ITA/Milan-UNIMI-1/2020	Matteo Iannacone; Fumagalli et al.[85,86]	GenBank: MT748758.1
Biological samples		
Human varicose veins	Thomas Korff	N/A
Human plasma from hospitalized COVID-19 patients with pneumonia of moderate severity	CORKUM at LMU	N/A
Chemicals, peptides, and recombinant proteins		
Cobra venom factor	Quidel	Cat#A600
Crry	Christoph Q. Schmidt and Arthur Dopler; Schmidt et al.[87]	N/A
Rhodamin B	Sigma-Aldrich	Cat#83689
Acridine orange	Sigma-Aldrich	Cat#318337
Fluorescein isothiocyanate–dextran (FITC-Dextran)	Sigma-Aldrich	Cat#74817
Pierce™ 16% Formaldehyde (w/v), Methanol-free	ThermoFisher	Cat#28908
Hoechst	ThermoFisher	Cat#H3570
Xylol	Merck	Cat#1082984000
Ethanol	Merck	Cat#1.00983
Citrate buffer (Citric acid monohydrate)	Sigma-Aldrich	N/A
Chrono-Lume	Probe&go	#70 210
Ala-Tyr-Pro-Gly-Lys-Phe-NH2 -trifluoracetat (PAR4 activator)	Sigma-Aldrich	#A3227
Tirofiban	Ibisqus GmbH	PZN 11312820
Fibrinogen	Enzyme research laboratory	# MFg
Chondroitin-sulfate A	Sigma-Aldrich	# C9819
Bovines Serumalbumin (BSA)	Carl Roth	# T844.1
Thrombin	Sigma-Aldrich	# T4648
Startem reagent	Tem Innovations	000503-10
Extem reagent	Tem Innovations	000503-05
Triton X-100	Sigma-Aldrich	Cat#X100
PBS (10X)	Gibco	Cat#70011-036
PBS (1X)	Gibco	Cat#14190-094
StemPro Accutase	Gibco	Cat#A1110501
FBS	Biosell	Cat#S 0613
EDTA	ThermoFisher	Cat#15575020

(*Continued on next page*)

Continued

REAGENT or RESOURCE	SOURCE	IDENTIFIER
Neuraminidase	Foresight biosciences	Cat#FSB0001_10
Chondroitinase ABC	Sigma-Aldrich	Cat#C3667
Heparinase III	Sigma-Aldrich	Cat#H8891
DPBS, calcium, magnesium (1x)	Gibco	Cat#14040117
Collagenase 1	Sigma-Aldrich	Cat#C0130
Collagenase 11	Sigma-Aldrich	Cat#C7657
Hyaluronidase	Sigma-Aldrich	Cat#D4527
DNase 1	Sigma-Aldrich	Cat#H3506
Collagenase 2	Worthington Biochemical	Cat#LS004174
Elastase	Worthington Biochemical	Cat#LS002292
Reverse Transcription System	Promega	Cat#A3500
SYBR® Green Master Mix	Bio-rad	Cat#1725150
Ficoll density gradient (Ficoll® Paque Plus; GE Healthcare)	Sigma-Aldrich	Cat#17-1440-02
RIPA Lysis and Extraction Buffer	ThermoFisher	Cat#89900
Pierce™ ECL Western Blotting Substrate	ThermoFisher	Cat#32106
Alexa Fluor (AF)-594 Phalloidin	Invitrogen	Cat#A12381
Aprotinin (Trasylol)	Nordic Pharma	PZN 11088647
Polylysin	EMD Millipore	Cat#A-005-C
TNP-conjugated BSA	Biosearch Technologies	Cat#T-5050-10
Critical commercial assays		
ELISA for IgM	Abcam	Cat#ab215085
ELISA for IgG	Abcam	Cat#ab151276
RNeasy Micro Kit	Qiagen	Cat#74004
Pierce™ BCA Protein Assay Kit	ThermoFisher	Cat#23225
Neutrophil Isolation Kit, mouse	Miltenyibiotec	Cat#130-097-658
Experimental models: Cell lines		
Mouse: C57BL/6 primary vein endothelial cells	Cell Biologics	Cat#C57-6009
Human: Umbilical Vein Endothelial Cells	PromoCell	Cat#C-12203
Human: Saphenous Vein Endothelial Cells	PromoCell	Cat#C-12231
Experimental models: Organisms/strains		
Mouse: C57BL/6	Jackson Laboratory	Cat#000664
Mouse: *Rag1*$^{-/-}$	Jackson Laboratory; Mombaerts et al.[88]	Cat#002216
Mouse: *Alb*$^{-/-}$	Jackson Laboratory; Roopenian et al.[89]	Cat#025201
Mouse: *Mbl1/2*$^{-/-}$	Jackson Laboratory; Shi et al.[90]	Cat#006122
Mouse: *Ighm*^{tm1Che}	Boes et al.[91]	Michael Carroll
Mouse: *Aicda*$^{-/-}$	Muramatsu et al.	Mark Suter
Mouse: *Aicda*$^{-/-}$*Ighm*^{tm1Che}	Kumazaki et al.[92]	Michael Carroll
Mouse: *C1q*$^{-/-}$	Botto et al.[93]	Marina Botto
Mouse: *Cfb*$^{-/-}$	Pekna et al.[94]	Marina Botto
Mouse: *C3*$^{-/-}$	Wessels et al.[95]	Michael Carroll
Mouse: *C4*$^{-/-}$	Fischer et al.[96]	Michael Carroll
Mouse: *C3ar1*$^{-/-}$	Fischer et al.[97]	Craig Gerard
Mouse: *C5*$^{-/-}$	Wetsel et al.[98]	N/A
Mouse: *B10.D2-Hc1 H2d H2-T18c/nSnJ*	Jackson Laboratory; Wetsel et al.[98]	Cat#000463
Mouse: *C5ar1*$^{-/-}$	Hopken et al.[99]	N/A

(*Continued on next page*)

Continued

REAGENT or RESOURCE	SOURCE	IDENTIFIER
Mouse: *Fcgr*$^{-/-}$*Fcgr2b*$^{-/-}$	Park et al.[100]; van Montfoort et al.[101]	Falk Nimmerjahn
Mouse: *Fcmr*$^{-/-}$	Lang et al.[102]	Karl Lang
Mouse: *Cr2*$^{-/-}$	Molina et al.[103]	Mark Zabel
Mouse: *KL25*	Hangartner et al.[39]	Hans Hengartner and Rolf Zinkernagel
Mouse: *Itgax*$^{-/-}$	Wu et al.[104]	Christie Ballantyne
Mouse: *Itgam*$^{-/-}$	Coxon et al.[105]	Siamon Gordon
Mouse: *Cμ13*	Rutemark et al.[106]	Birgitta Heyman
Mouse: *Pf4Cre/Rosa-Yfp*	Tiedt et al.[107]	N/A
Mouse: *Fcgr2a*	McKenzie et al.[108]	N/A
Mouse: *VeCdhCreFcmrfl/fl*	Chen et al.[109]; da Palma Guerreiro et al.[110]	This paper
Mouse: *K18-hACE2*	Jackson Laboratory McCray et al.[111]	Cat#034860
Mouse: *Fcmr*$^{fl/fl}$	da Palma Guerreiro et al.[110]	Alexandra da Palma Guerreiro and Lukas P. Frenzel
Oligonucleotides		
Mm_Faim3_1_SG QuantiTect Primer Assay	Qiagen	#QT01066842
Mm_Pigr_1_SG QuantiTect Primer Assay	Qiagen	#QT00165046
FcαμR CF: CTCCCTTTCAGGTACAAATGCA	Eurofins genomics, Germany	N/A
FcαμR CR: TCTGTGGAACGTCAGTGAGAGC	Eurofins genomics, Germany	N/A
Hs_FAIM3_1_SG QuantiTect Primer Assay	Qiagen	#QT00011221
Software and algorithms		
AxioVision software	Zeiss	Version 4.8
FlowJo	BD Biosciences	Version 10
ZEN software	Zeiss	Version 2.3
ImageJ software (U. S. National Institutes of Health, Bethesda, Maryland, USA).	FIJI	Version 2.9.0
R package "corrplot"	https://github.com/taiyun/corrplot	Version 0.84

EXPERIMENTAL MODEL AND STUDY PARTICIPANT DETAILS

Animals

C57BL/6, *Rag1*$^{-/-}$,[88] *Alb*$^{-/-}$,[89] and *Mbl1/2*$^{-/-}$[90] mice were obtained from Jackson and generated as described. *Ighm*^{tm1Che},[91] *Aicda*$^{-/-}$, *Aicda*$^{-/-}$*Ighm*^{tm1Che},[92] *C1q*$^{-/-}$,[93] *Cfb*$^{-/-}$,[94] *C3*$^{-/-}$,[95] *C4*$^{-/-}$,[96] *C3ar1*$^{-/-}$,[97] *C5*$^{-/-}$ and B10.D2-Hc1 H2d H2-T18c/nSnJ control mice,[98] *C5ar1*$^{-/-}$[99] *Fcgr*$^{-/-}$*Fcgr2b*$^{-/-}$,[100,101] *Fcmr*$^{-/-}$,[102] *Cr2*$^{-/-}$,[103] *KL25*,[39] *Itgax*$^{-/-}$,[104] *Itgam*$^{-/-}$,[105] *Cμ13*,[106] *Pf4Cre/Rosa-Yfp*,[107] *Fcgr2a*,[108] *VeCdhCreFcmr*$^{fl/fl}$,[109,110] and K18-hACE2 mice[111] were generated as described (see Table S1). Mice were kept at 55% humidity and 21°C temperature with a 12h day-night rhythm. Further details are provided in the method details. All procedures performed on mice were approved by the local legislation on protection of animals (Regierung von Oberbayern, Munich).

Generation of *Fcmr*$^{fl/fl}$ mice

Fcmr-floxed C57BL/6 mice were generated by TaconicArtemis (Cologne, Germany) via flanking Exons 2, 3 and 4 with loxP sites.

Endothelial cell culture

C57BL/6 mouse primary vein endothelial cells (MVEC, (#C57-6009, Cell Biologics) isolated from inferior vena cava tissue of mice were cultured in tissue culture flasks pre-coated with gelatin-based coating solution in culture complete growth medium (#M1168, Cell Biologics). Human Umbilical Vein Endothelial Cells (HUVEC, #C-12203, PromoCell) and Human Saphenous Vein Endothelial Cells (HSaVEC, #C-12231, PromoCell) were cultured in tissue culture flasks pre-coated with gelatin-based coating solution in Endothelial Cell Growth Medium (#C-22010, PromoCell). All endothelial cells were cultured in a humidified incubator at 37°C and 5% CO_2.

Human thrombi and veins

Great saphenous veins were collected from patients after informed consent undergoing excision of varicose veins (CEAP (clinical, etiological, anatomical, pathological) classification C2–C3) or removal of healthy veins for bypass surgeries. Pulmonary thrombectomy specimens were obtained during surgeries and contained fresh thrombotic parts. Collection was covered by a waiver from the institutional review board for the anonymous use of leftover material. Immunofluorescence staining was performed on paraffin-embedded lungs of patient, who died from PCR test confirmed SARS-CoV infection. Specimens were collected in agreement with the local ethics committee (Heidelberg University and Ludwig-Maximilians University, respectively) and conformed to the principles outlined in the Declaration of Helsinki.

METHOD DETAILS

Mouse model of flow restriction in the IVC

After a median laparotomy the IVC was exposed, and a space holder was positioned followed by a narrowing ligature. Subsequently, the wire was removed to avoid complete vessel occlusion. Side branches were not ligated or manipulated. All groups were age, sex, and weight matched. Mice between the age of 18 and 22 weeks were included in the analysis. Mice with bleedings or any injury of the IVC during surgery were excluded from further analysis. For thrombus weight measurement after 48 hours, the IVC was excised just below the renal veins and proximal to the confluence of the common iliac veins. A C1q depleting Ab (200 μg, RmC 7H8. rat IgG1) was injected i.v. 12 hours before surgery, cobra venom factor for C3 depletion (50 μg, Quidel) was injected i.p. 16 hours (50 μg) and 1 hour (25 μg) prior to surgery, Crry (500μg i.v.) 2 hours before surgery followed by every 12 hours, and isotype rat IgG1 (200 μg, TNP6A7, bioxcell) or PBS served as control. Serum from C57Bl6 mice was injected i.v. 48 and 24 hours prior to surgery (250 μl each). Mouse pooled polyclonal IgM (600 μg, Rockland), pooled polyclonal IgG (600 μg, Jackson Immuno Research), mouse monoclonal anti-influenza A virus NP IgG2a (600μg, H16-L10-4R5 (HB65), BioXcell), mouse monoclonal anti-HIV gp120 IgG1 (600 μg, 55-36, BioXcell), mouse monoclonal anti-KLH IgM (200 μg, BioXcell), or mouse Fc-Fragment (600 μg, BioXcell) were injected i.v. immediately before surgery. Platelet depletion was induced using a rat anti-mouse GPIbα (CD42b) Ab i.v. (2 mg/kg body weight, Emfret analytics) or a rat isotype IgG together with pooled polyclonal IgG (600 μg, Jackson Immuno Research). A mouse anti-FITC IgG1 Fc silent or control Ab with normal Fc part (600 μg i.v. 4-4-20, absolute Ab) was administered immediately before surgery. A pIgR inhibitor antibody (10μg, ab170321, abcam) or isotype control (10μg, BE0290, Bioxcell) were injected i.v. to *C57Bl6*, *Fcmr*$^{-/-}$ or *VeCdhCreFcmr*$^{fl/fl}$ mice 1 hour before ligation.[33] Mouse monoclonal anti-HIV gp120 IgG1 (monomeric or aggregates) (600 μg, 55-36, BioXcell) was injected i.v. to *Ighm*^{tm1Che} mice 1 hour before ligation. Mouse monoclonal anti-HIV gp120 IgG1 heat aggregates were obtained by incubating the antibodies at a concentration of 20mg/ml at 63°C for 30 minutes. *Aicda*$^{-/-}$*Ighm*^{tm1Che} mice were injected i.v. with 600μg of mouse IgG1 anti-TNP non-complement activating antibody H5 mAb (B8401H5) or a mouse IgG1 Isotype control (BE0083, Bioxcell) 1 hour before ligation. Blood cell counts were determined using an automated cell counter (Sysmex).

Microvascular thrombosis model

Using intravital microscopy we investigated phototoxic injury-induced thrombus formation in exteriorized cremaster muscle postcapillary venules as described before.[112] Briefly, after anesthetizing male mice (125 mg/kg ketamine 25 mg/kg xylazine i.p.) and placing them on a heating plate, the carotid artery was cannulated and the right cremaster muscle was surgically prepared and exteriorized for intravital microscopy. Appropriate cremaster muscle postcapillary venules were then microscopically identified. Phototoxic injury in venules was induced by injection of 2,5% FITC-Dextran (1,5μL/g bodyweight) in 0,9% NaCl solution and subsequent exposure of postcapillary venules to a high intensity light source (Olympus BX51, mercury lamp, Hamburg, Germany). Measurement of microvascular blood flow velocities was conducted using a dual photodiode and a digital on-line cross-correlation program (Circusoft Instrumentation).

Intravital epifluorescence microscopy

Murine platelets were isolated from whole blood and labeled with Rhodamin B.[113] For quantification of leukocyte adhesion, acridine orange (Sigma-Aldrich) was injected i.v. Imaging was performed with an Olympus BX51WI microscope using a 20x (NA 0.95) water immersion objective and an ORCA-ER CCD Camera (Hamamatsu). Cell recruitment was quantified in four fields of view (50x100μm) per animal before and at different timepoints after IVC stenosis: immotile cells were counted as adherent. The cell covered area (mm^2) and colocalization area were determined by planimetric measurement.

Immunofluorescence staining of frozen and paraffin embedded sections

The IVC was embedded in OCT, stored at -80°C and cut with a cryotome (CryoStar NX70 Kryostat, ThermoFisher Scientific) into 5 μm slices, fixed with 4% formaldehyde, and blocked with the respective serum. Sections were incubated with primary Ab for CD41 (clone: MWReg30, BD Bioscience; #12-0411-83; isotype: rat IgG1), Fibrin(-ogen) (clone: polyclonal; DAKO; #A0080; isotype: rabbit IgG), Ly6G (clone: 1A8, ThermoFisher; #12-9668-82; isotype: rat IgG2a), MPO (clone: polyclonal; DAKO; #A0398; isotype: rabbit IgG), F4/80 (clone: CI:A3-1, AbD Serotec; #MCA497; isotype: rat IgG2b), C4 (clone: 16D2; ThermoFisher; #MA1-40047; isotype: rat IgG2a),

CD42b (clone: polyclonal, Abcam; #ab104704; isotype: rabbit IgG), IgM heavy chain (clone: polyclonal, ThermoFisher; #A21042; Isotype: goat IgG), FcμR (clone: polyclonal; Sigma aldrich; #HPA003910; Isotype: rabbit IgG), C1q (clone: RmC 7H8; isotype: rat IgG1), vWF (clone: polyclonal; Dako; #A0082; isotype: rabbit IgG), CD62P (clone: RB40.34 (RUO); BD Biosciences; #553742; isotype: rat IgG1, λ), ICAM1 (clone: 020; Sino biological, #50440-R020, Isotype: rabbit IgG), and CD31 (clone: 390, ThermoFisher; #16-0311-85; Isotype: rat IgG2a, kappa). Alexa labeled secondary Ab (Invitrogen) were used for detection. In order to avoid unspecific staining Alexa labeled F(ab)2-fragments against mouse IgG Fcγ (clone: Polyclonal; Jackson Immunoresearch; # 115-546-071; Isotype: goat F(ab)2-fragments) were used. By staining *Aicda*$^{-/-}$ thrombi, no FITC signal could be detected, confirming the specificity of staining. DNA staining was performed using Hoechst (ThermoFisher; #H3570). Image acquisition was carried out by using a Zeiss Axio imager microscope with an AxioCam. For quantification of NETS three criteria had to be fulfilled: (1) Presence of extracellular DNA protrusions, (2) the protrusion has to originate from a Ly6G-marked cell, (3) the DNA-structure has to be decorated by MPO. Human samples were paraffin fixed. The slides were first treated with Xylol (Merck; #1082984000) and descending concentration of ethanol (Merck; #1.00983). Then the slides we boiled in 2%, citrate buffer (Citric acid monohydrate, Sigma-Aldrich). In order to avoid unspecific staining, we used primary labeled F(ab)2-fragments to detect human IgG-Fc (clone: polyclonal; Abcam; ab98593; Isotype: goat F(ab')2). To ensure specific staining, we used DyLight-conjugated goat anti rat IgG Ab as control (clone: polyclonal; ThermoFisher; #SA5-10021). The following primary Ab have been used for human specimens: CD42b (clone: 42C01; ThermoFisher; #MA5-11642; Isotype: mouse IgG), C4 (clone: polyclonal; Bioss; # bs-15186R-A647; Isotype: rabbit IgG), C1q (clone: polyclonal; Bioss; # bs-10750R-A647 or # bs-10750R-A488; Isotype: rabbit IgG), C3 (clone: polyclonal; Bioss; bs0367G-A647, Isotype: goat IgG), and CD31 (clone: JC/70A; ThermoFisher; #MA5-13188; Isotype: mouse IgG). To measure fluorescent area or intensity AxioVision software (Zeiss) was used.

Light transmission aggregometry

Platelet aggregation essays were performed on an optical-/lumi-aggregometer (model 700, CHRONO-LOG®). Blood samples were taken by intracardiac puncture and subsequent anticoagulation with heparin. Platelet rich plasma was obtained by centrifugation at 70g for 20 minutes; Platelet poor plasma was gained by re-centrifugation at 1800g for 10 minutes. ATP-release was measured by adding 1,6x10-2mg/ml luciferin and 1760U/ml luciferase (Probe&go) and calibrated with 1nmol ATP (Probe&go). Aggregation was induced using 200 μmol/l PAR4 activator (Sigma-Aldrich). Investigation of Ab mediated complement activation and Ab substitution was achieved by adding Fc-silent or Fc-WT Ab directed against fluorescein (clone: 4-4-20; absolute antibody, #Ab00102-1.4, and #Ab00102-1.1, Isotype: mouse IgG1).

Flow cytometry of platelet-antibody interaction

Blood samples were gained as described above and anticoagulated by acid-citrate-dextrose. To isolate washed platelets, PRP was centrifuged at 1200g for 10 minutes. Assays were carried out using a flow cytometer (Gallios, Beckman Coulter). In order to study interactions between Ab and platelets we focused on FITC labeled IgM isotype control (clone: G155-228 (RUO), BD Biosciences, #553474) and IgG1 isotype control (clone: MOPC-31C (RUO), BD Biosciences, #550616) as well as on Fc silent and Fc wildtype anti-FITC (clone: 4-4-20; absolute antibody, #Ab00102-1.4, und #Ab00102-1.1; Isotype: mouse IgG1) which were labeled by Alexa 488 (ThermoFisher scientific, Waltham, USA, Isotype: mouse IgG2a). The Ab concentration in the experiments was $7.5x10^{-3}$ mg/ml. The incubation time of Ab was six minutes before platelet activation. Tirofiban (Ibisqus GmbH,) was used at 1.2 μg/ml. Platelet aggregation after application of 100 μmol/l PAR4 activator (Sigma-Aldrich, #A3227) was monitored by forward and side scatter, platelet activation was assesses using a rat anti-mouse CD62P Ab (Clone RB40.34, BD Biosciences, #563674; Isotype: Rat IgG1). For human platelets an anti-CD62P Ab (clone: CLB-Thromb/6, Immunotech a coulter company, #1759, Isotype: mouse IgG1) was used together with a human isotype control IgG (clone: polyclonal, antikoerper-online.de, #ABIN964314). All samples were analyzed using LSRFortessa flow cytometer (BD Biosciences) and data were interpreted using FlowJo Software.

Antibody deposition assay

Experiments were performed on a Tecan infinite 200 ELISA reader using flat-bottom well plates (Thermo Fisher scientific). To investigate Ab deposition on different components of the thrombus fibrinogen (1 mg/ml, Enzyme research laboratory), chondroitin-sulfate A (1 mg/ml, Sigma-Aldrich), or albumin (1 mg/ml, Carl Roth) were coated on well plates. Fibrin was produced by adding 0,5U Thrombin (Sigma-Aldrich) together with calcium and magnesium. Blood plasma and platelets were isolated by intracardiac puncture and two centrifugation steps as described previously. Ab deposition was analyzed by adding a FITC labeled IgG1 isotype control (BD Biosciences) in plasma or tyrode's buffer, followed by centrifugation and washing with tyrode's buffer.

Enzyme-linked Immunosorbent Assay

ELISA for IgM (abcam, ab215085) and IgG (abcam, ab151276) were performed according to the instructions of the manufacturer.

Thromboelastometry

Citrated whole blood from mice was recalcified for extem measurements by adding startem reagent, while the coagulation was initiated by extem reagent (Tem Innovations). In fibtem measurements platelets were inactivated via cytochalasin D. For analysis a rotation thromboelastometry device was used (ROTEG®05, Pentapharm).

Tail bleeding assay

After anesthesia with buprenorphine and isoflurane the tail was incised 5 mm from the tip. The bleeding tail was placed on Whatman paper and the time until bleeding stopped was measured.

Endothelial cell culture

C57BL/6 mouse primary vein endothelial cells (MVEC, (#C57-6009, Cell Biologics) isolated from inferior vena cava tissue of mice were cultured as described above. Ab binding to MVECs was assessed after incubation with a FITC-labeled mouse isotype IgG1 (clone: MOPC-31C; BD Bioscience; #550616) or FITC-labeled mouse isotype IgM (clone: G155-228; BD Bioscience; #553474). After incubation of the MVEC for 1 hour with FITC-labeled isotype IgG1, IgM (50μg/mL both), or cell culture medium, cells were washed twice with PBS and fixed in 4% formaldehyde. Cells were then permeabilized with 0.1% Triton X-100 and stained with Alexa Fluor (AF)-594 phalloidin (#A12381, Invitrogen). Cells were then washed and stained with Hoechst 33342. vWF and P-selectin immunostainings were performed on MVEC incubated for 1 hour with FITC-labeled isotype IgG1, IgM (50μg/mL both), or cell culture medium. After washing and fixation in 4% formaldehyde, cells were saturated in 10% goat serum for 1 hour. Cells were incubated with rabbit anti-mouse vWF (clone: polyclonal; Dako; #A0082; isotype: rabbit polyclonal IgG) or P-selectin (clone: polyclonal; biorbyt; #orb385621; isotype: rabbit polyclonal IgG) primary Ab, and stained with Alexa Fluor 594 conjugated secondary Ab (Invitrogen). Nuclei were stained with Hoechst 33342 (Invitrogen). Images were acquired with Zeiss Laser Scanning Microscope LSM 880 with an Airyscan module (Carl Zeiss Microscopy) and processed using ZEN software (Zeiss). Staining intensity was quantified using ImageJ software (U. S. National Institutes of Health, Bethesda, Maryland, USA).

For the pIgR blocking antibody experiments under static conditions, MVECs were cultured as described above. The pIgR blocking antibody (50μg/mL, #AF2800, R&D Systems) or isotype control (Polyclonal Goat IgG) were added to the medium for 1 hour prior to the incubation of cells for 1 additional hour with the FITC-labeled mouse isotype IgM.

Human Umbilical Vein Endothelial Cells (HUVEC, #C-12203, PromoCell) and Human Saphenous Vein Endothelial Cells (HSaVEC, #C-12231, PromoCell) were cultured under static conditions as described above.

Flow cytometry of MVECs

To assess the binding of the isotype IgG1 and IgM to the MVEC with flow cytometry, cells were incubated for 1 hour with FITC-labeled isotype IgG1 (clone: MOPC-31C; BD Bioscience; #550616), isotype IgM (clone: G155-228; BD Bioscience; #553474) (50μg/mL), a FITC-labeled anti-ICAM-1 Ab (clone: Clone 3E2; BD Bioscience; #561898), or PBS. Cells were washed twice with PBS and detached from the tissue culture wells using StemPro Accutase (#A1110501, Gibco). The enzymatic activity of the Accutase was disabled with PBS supplemented with 10% FBS. Cells were then washed twice with PBS supplemented with BSA (0.5%) and EDTA (2mM) and analyzed by flow cytometry. The binding of the isotype IgM to the MVEC after the disruption of the glycocalyx was assessed after treatment of cells for 1 hour with neuraminidase (1U/mL, #FSB0001_10, Foresight biosciences), chondroitinase ABC (1U/mL, #C3667, Sigma), and heparinase III (5U/mL, #H8891, Sigma). All samples were analyzed using LSRFortessa flow cytometer (BD Biosciences) and data were interpreted using FlowJo Software.

Flow cytometry for Fcμ Receptor expression on HUVECs and HSaVECs

To assess the expression of the human FcμR on the surface of HUVECs and HSaVECs from early passage (P4 to 6) were cultured under static conditions as described before. Cells were washed twice with PBS and detached from the tissue culture wells using StemPro Accutase (#A1110501, Gibco). The enzymatic activity of the Accutase was disabled with PBS supplemented with 10% FBS. Cells were then washed twice with PBS supplemented with BSA (0.5%) and EDTA (2mM). Cells were stained with PE Mouse anti-Human Fcμ Receptor (clone: HM14-1, BD Bioscience; #563017) or PE Mouse IgG1, κ Isotype Control (clone: MOPC-31C; BD Bioscience; #550617) and analyzed by flow cytometry as described before.

Chimera generation

6 x 10^6 bone marrow cells from donor mice were injected into the tail vein of irradiated (900 rad) recipient mice. 8 weeks after transplantation thrombus formation was induced in bone marrow reconstituted mice.

Proteome analysis

Plasma proteome of longitudinally sampled COVID-19 patients was used for complement factor correlations. For detailed methods on the plasma protein mass spectrometry and profiling see Pekayvaz et al.[114] Correlations between plasma protein expression and/or D-Dimer were computed and visualized with R using corrplot (Taiyun Wei and Viliam Simko (2017). R package "corrplot": Visualization of a Correlation Matrix (Version 0.84). https://github.com/taiyun/corrplot). D-Dimer data was available for 25 time points of 11 patients (hospitalized COVID-19 patients with pneumonia of moderate severity, WHO clinical progression score 4-5), as was plasma protein expression. In cases of D-Dimer at or below the detection threshold (0.5μg/ml), this value was used as a minimum value. The

mean protein expression was used to calculate the scores using the following proteins respectively: Classical pathway (CP) score, terminal pathway (TP) score, lectin pathway (LP) score, alternative pathway (AP) score:

CP Score	C1QA	C1QB	C1QC	C1R	C1S	C4A	C4B	C2	C3
LP Score					MASP1	MASP2	MBL2		
AP Score	CFP	CFD							
TP Score	C5	C6	C7	C8A	C8B	C8G	C9		
IgG Score	IGHG1	IGHG2	IGHG3	IGHG4					
Ig Score	IGHG1	IGHG2	IGHG3	IGHG4	IGHD	IGHE	IGHM		

P values, indicating slope significantly non-zero, are displayed as *p<0.05, **p<0.01, ***p<0.001. Positive correlations are shown in blue and negative correlations in red. Color intensity and the size of the ellipse are proportional to the correlation coefficient.

Flow chamber experiments

C57BL/6 mouse primary vein endothelial cells (MVEC) (#C57-6009, Cell Biologics) from early passages were seeded in flow chamber slides (μ-slide I Luer 0.4 mm; #80176; Ibidi): 1.8 x 10^5 cells in 100μl of culture complete growth medium (#M1168, Cell Biologics) per slide. After 2 hours of incubation in a humidified incubator at 37°C and 5% CO_2 cells were attached and slides were connected to fluidic units (#10902, Ibidi). Assembly of fluidic units to an air-driven flow pump system (#10902, Ibidi) allowed perfusion of cells with continuous laminar flow under cell culture conditions. Complete growth medium was perfused in the slides for 24 hours with a shear stress of 10 dyn/cm^2 simulating the physiological condition in the murine IVC.[115] This was followed by perfusion of 3 independent slides with 3 different shear stress values of 10, 5 and 0,5 dyn/cm^2 for another 2 hours mimicking the stasis condition after the partial flow reduction in the IVC. IgM binding to MVECs under these different flow conditions was assessed after incubation of cells for 1 additional hour with a FITC-labeled mouse isotype IgM (12.5μg/mL, clone: G155-228, #553474; BD Bioscience). Cells were then washed, fixed, permeabilized, and stained with Alexa Fluor (AF)-594 phalloidin and Hoechst as described before. Images were acquired with Zeiss Laser Scanning Microscope LSM 880 with an Airyscan module (Carl Zeiss Microscopy) and processed using ZEN software (Zeiss). Immunofluorescence intensity was quantified using ImageJ.

For the pIgR blocking antibody experiments under flow conditions, MVEC were cultured under flow conditions as described above. The pIgR blocking antibody (50μg/mL, #AF2800, R&D Systems) or isotype control (Polyclonal Goat IgG), were added to the medium during the 2 hours reduced flow incubation time prior to the incubation of cells for the 1 additional hour with the FITC-labeled mouse isotype IgM. IgM binding quantifications, and vWF and P-selectin immunostainings and quantifications were performed as described before.

rtPCR

C57BL/6 mouse primary vein endothelial cells (MVEC) (#C57-6009, Cell Biologics) from early passage (P4 to 6), were cultured as described before. C57Bl6, *Fcmr*$^{-/-}$ or B cell deficient *Rah1*$^{-/-}$ mice were perfused by intracardiac puncture with PBS containing CaCl2 and MgCl2 (Gibco). IVC, kidney, spleen and liver were collected and washed in PBS containing CaCl2 and MgCl2. IVCs were then incubated successively at 37°C in two different enzyme mixes: (a) collagenase 1, collagenase 11, Hyaluronidase, DNase 1; and (b) collagenase 2 and Elastase; for 15 and 40 minutes respectively. To obtain a uniform single-cell suspension from tissues, 70 μm nylon cell strainers were used. RNA was extracted using the RNeasy Micro Kit (#74004; Qiagen). Reverse transcription was performed using 2μg RNA per sample with "Reverse Transcription System" (#A3500, Promega). qRT-PCR was performed using the SYBR® Green Master Mix (Bio-rad) on a Biorad iCycler. The following primers were used for the detection of the expression of the murine FcμR "Mm_Faim3_1_SG QuantiTect Primer Assay" (#QT01066842, Qiagen), pIgR "Mm_Pigr_1_SG QuantiTect Primer Assay" (#QT00165046, Qiagen) and FcαμR CF: CTCCCTTTCAGGTACAAATGCA; CR: TCTGTGGAACGTCAGTGAGAGC (eurofins genomics, Germany).[116]

rtPCR for IgM receptors in endothelial cells

To assess the expression of FcμR, pIgR and FcαμR receptors in MVEC under flow conditions, the C57BL/6 mouse primary vein endothelial cells (MVEC) from early passage (P4 to 6) were seeded in flow chamber slides (μ-slide I Luer 0.4 mm; #80176; Ibidi) and then perfused with complete growth medium for 24 hours with a shear stress of 10 dyn/cm^2 simulating the physiological condition in the murine IVC as described before. This was followed by perfusion of different slides with complete growth medium with two different shear stress values of 10 or 0,5 dyn/cm^2 for another two hours mimicking the stasis condition after the partial flow reduction in the IVC. MVEC were then detached and isolated from the flow chamber using StemPro Accutase as described before. The RNA extraction, reverse transcription and qRT-PCR were performed as described before. The following primers were used for the detection of the expression of the murine FcμR "Mm_Faim3_1_SG QuantiTect Primer Assay" (#QT01066842, Qiagen), pIgR "Mm_Pigr_1_SG QuantiTect Primer Assay" (#QT00165046, Qiagen) and FcαμR CF: CTCCCTTTCAGGTACAAATGCA; CR: TCTGTGGAACGTCAGTGAGAGC (eurofins genomics, Germany).[116]

rtPCR for Fcμ Receptor in HUVEC and HSaVEC under static conditions. HUVECs and HSaVECs from early passage (P4 to 6) were cultured under static conditions as described before. The RNA extraction, reverse transcription and qRT-PCR were performed as described before. The following primer was used for the detection of the expression of the human FcμR: "Hs_FAIM3_1_SG QuantiTect Primer Assay" (#QT00011221, Qiagen).

Western Blot

C57BL/6 mouse primary vein endothelial cells (MVEC) (#C57-6009, Cell Biologics) from early passage (P4 to 6), were cultured as described before. Murine blood samples were taken by intracardiac puncture and subsequent anticoagulation with citrate. PBMC cells were isolated by Ficoll density gradient (Ficoll® Paque Plus; GE Healthcare; #17-1440-02; Sigma). Diluted blood with PBS (1:1) was layered on half volume of Ficoll, centrifuged for 30 minutes at 400g. PBMC layer was then collected and washed twice with PBS. Cells were lysed in RIPA Lysis and Extraction Buffer (#89900; ThermoFisher). Cell lysates were cleared by centrifugation and supernatant fractions were used for Western blot. Total protein concentration was measured (Pierce™ BCA Protein Assay Kit; #23225; ThermoFisher) and the equal amount of 40μg of proteins was used per sample for each assay. Cell lysates were resolved by SDS-PAGE and transferred to nitrocellulose membranes (ThermoFisher). Blots were probed overnight at 4°C with the FcμR Ab (FAIM3 Polyclonal Ab; 1:500, #bs-7527R; Bioss), and then probed with secondary HRP-linked Ab (1:5000) for 1 hour at room temperature. Binding of the Ab to the blots was detected using a "Pierce™ ECL Western Blotting Substrate" (#32106; ThermoFisher). The signal was revealed using a CURIX 60 X-ray film processor (AGFA).

Recombinant expression and purification of the murine complement inhibitor Crry

A codon optimized gene coding for the amino acid sequence of a soluble form of murine Crry (Uniprot Q64735 amino acids 64-400) was ordered from Geneart. Potential N-glycosylation sites were removed by changing the consensus sequence of 'NXS/T' to 'QXS/T'. The obtained coding sequence for Crry was subcloned into the yeast expression vector pPICZaB (Invitrogen), using PstI and XbaI restriction enzyme (New England Biolabs) sites, downstream of the alcohol oxidase (AOX1) promoter and behind the DNA coding for the prepro-alpha-factor secretion signal. Subsequently KM71H *P. pastoris* cells (Invitrogen) were transformed with Sac I-linearised plasmid (using electroporation and standard settings on a Biorad GenePulser). Selection of *P. pastoris* clones containing the expression plasmid was achieved by streaking transformed yeast onto YPDS (i.e. 1% (w/v) yeast extract, 2% (w/v) peptone, 2% (w/v) dextrose, 1 M D-sorbitol) plates containing 300 mg/ml Zeocin. One of the cell colonies that grew (30°C for three-four days) on these antibiotic-containing plates was selected for protein expression.

Large-scale protein production was performed by high cell density fermentation using a Minifors (from INFORS HT) bioreactor equipped with a 5-l cylindrical fermentor vessel following the expression protocol as detailed in a previous report with small modifications.[87]

Protein capture and purification was performed after centrifugation and filtration (0.22 μm filter) to remove cells and after addition of EDTA and PMSF to final concentrations of 5 and 0.5 mM as well as 3 protease inhibitor cocktail tablets (cOmplete ULTRA tablets from Roche). The fermentor supernatant was diluted one-in-five with distilled water with the pH being adjusted to 4.0 prior to application to a prepacked PorosHS column (from Applied Biosystems) using the sample pump of an NGC medium-pressure chromatography systems (from BioRad). After washing with equilibration buffer (sodium acetate buffer at pH 4.0 containing 5 mM EDTA), elution was achieved by applying a linear towards the same buffer that had been supplemented with 1M NaCl. Fractions containing protein were pooled and submitted to further purification which included i) a high resolution cation exchange chromatography utilizing a MonoS column (GE life sciences) at pH 5.0, ii) size exclusion chromatography step using a HiLoad Superdex 26/600 200 pg column (GE life sciences) equilibrated in PBS and finally iii) reversed phase chromatography step utilizing a ReproSil-XR 300 C4, 5 μm; 250 mm x 10 mm column (Dr. Maisch) on which the protein was loaded in PBS and elution was achieved by applying a linear gradient from aqua ad iniectabilia supplemented with 0.1 % TFA to a solution containing 70 % acetonitrile in aqua ad iniectabilia supplemented 0.085 % TFA (*data not shown*). Fractions containing very poor Crry were pooled and shock frozen in liquid nitrogen. The frozen protein pellet was lyophilized and dissolved in sterile, endotoxin free PBS. Relative absence of endotoxins (less than 0.05 EU/ml) was confirmed measuring the endotoxin concentrations of the re-constituted protein by EndoLISA® (from Hyglos GmbH).

NETosis assay

To isolate platelets and neutrophils citrated whole blood was collected by cardiac puncture from mice. Neutrophils were purified from whole blood using an isolation kit (miltenyi biotec, #130-097-658). To analyze the impact of complement components and platelets on the appearance of NETs, platelet-rich plasma was collected by centrifugation for 20 min at 70g. To maintain proportions, close to those *in vivo*, we used a platelet neutrophil ratio of 200:1. Final platelet concentration was titrated to 150.000/μl. To stabilize DNA 20 μg/ml aprotinin was added to the solution. To obtain balanced electrolyte concentrations calcium and magnesium were substituted to reach physiologic concentrations (1mmol/l). Platelets were stimulated by a PAR4-activator (Ala-Tyr-Pro-Gly-Lys-Phe-NH2 trifluoroacetate salt; 0,68g/l, #A3227-1MG, Sigma Aldrich). The coincubation of platelets and neutrophils were performed in eight well chambers (Nunc® Lab-Tek® II - CC2™ Chamber Slide™ system 8 wells, #S6815, Merck) covered with Polylysin (#A-005-C, EMD Millipore) for 3 hours at 37°C in a 5% CO2-atmosphere. Then the samples were fixed with 4% formaldehyde for 6 minutes. For NET detection DNA was stained with Hoechst 33342 (Invitrogen) combined with MPO (DAKO; #A0398; isotype: rabbit IgG). Image acquisition was carried out by using a Zeiss Axio imager microscope with an AxioCam.

SARS-CoV-2 infection mouse model combined with C1q and C3 complement component depletion

The SARS-CoV-2 infection mouse model was performed as previously described.[85,86] C1q depleting Ab (200 μg, RmC 7H8. rat IgG1) was injected i.v. and cobra venom factor for C3 depletion (50 μg, Quidel) was injected i.p. at different time points as described in the scheme in in Figure S5G. Isotype rat IgG1 (200 μg, TNP6A7, bioxcell) or PBS served as control.

Interaction of murine IgG immune complexes with FcμR-GFP Hek cells

IgG-IC were generated from TNP-conjugated BSA (TNP-33-BSA, Biosearch Technologies) and TNP-specific murine IgG1 (clone 7B4). 10μg/ml of IgG-IC were incubated with 100,000 cells for 60min at 60rpm on ice. After removal of unbound complexes by washing, cells were incubated with PE-conjugated goat anti-mouse IgG-Fc F(ab)2 (Jackson Immunoresearch) to detect bound IgG-IC on a BD flow cytometry CantoII instrument. Median fluorescence intensities were quantified and background binding to non-Toso expressing cells was subtracted from binding to FcμR expressing cells to obtain ΔMFI.

QUANTIFICATION AND STATISTICAL ANALYSIS

All data are shown as mean ± s.e.m. unless indicated otherwise. Experiments were analyzed using two-tailed unpaired two-sample t-test, paired t-test, ANOVA followed by LSD-post hoc-test, Tukey's Multiple Comparison Test, or Fisher exact test as indicated. A value of $P<0.05$ was considered significant. All analyses were performed using SigmaPlot or GraphPad.